JBC ARTICLE

The mitochondrial metal transporters mitoferrin1 and mitoferrin2 are required for liver regeneration and cell proliferation in mice

Received for publication, February 26, 2020, and in revised form, June 4, 2020 Published, Papers in Press, June 9, 2020, DOI 10.1074/jbc.RA120.013229

Alexandra Seguin[1,‡], Xuan Jia[1,‡], Aubree M. Earl[1], Liangtao Li[1], Jared Wallace[1], Andong Qiu[2], Thomas Bradley[1], Rishna Shrestha[1], Marie-Bérengère Troadec[3,4], Matt Hockin[5], Simon Titen[5], Dave E. Warner[1], P. Tom Dowdle[1], Martin E. Wohlfahrt[6], Elaine Hillas[7], Matthew A. Firpo[7], John D. Phillips[8], Jerry Kaplan[1], Barry H. Paw[9,†], Jonathan Barasch[2], and Diane M. Ward[1,*]

From the [1]Department of Pathology, University of Utah School of Medicine, Salt Lake City, Utah, USA, the [2]Columbia University, New York, New York, USA, the [3]University Brest, Inserm, EFS, UMR 1078, GGB, F-29200 Brest, France, [4]CHRU Brest, Service of Genetics, Laboratory of Chromosome Genetics, Brest, France, the [5]Department of Human Genetics and [6]Clinical Research Division, Fred Hutchinson Cancer Research Center, Seattle, Washington, USA, the Departments of [7]General Surgery and [8]Medicine, University of Utah School of Medicine, Salt Lake City, Utah, USA, and the [9]Harvard Medical School, Children's Hospital, Boston, Massachusetts, USA

Edited by Ursula Jakob

Mitochondrial iron import is essential for iron–sulfur cluster formation and heme biosynthesis. Two nuclear-encoded vertebrate mitochondrial high-affinity iron importers, mitoferrin1 (Mfrn1) and Mfrn2, have been identified in mammals. In mice, the gene encoding Mfrn1, *solute carrier family 25 member 37* (*Slc25a37*), is highly expressed in sites of erythropoiesis, and whole-body *Slc25a37* deletion leads to lethality. Here, we report that mice with a deletion of *Slc25a28* (encoding Mfrn2) are born at expected Mendelian ratios, but show decreased male fertility due to reduced sperm numbers and sperm motility. *Mfrn2*$^{-/-}$ mice placed on a low-iron diet exhibited reduced mitochondrial manganese, cobalt, and zinc levels, but not reduced iron. Hepatocyte-specific loss of *Slc25a37* (encoding Mfrn1) in *Mfrn2*$^{-/-}$ mice did not affect animal viability, but resulted in a 40% reduction in mitochondrial iron and reduced levels of oxidative phosphorylation proteins. Placing animals on a low-iron diet exaggerated the reduction in mitochondrial iron observed in liver-specific *Mfrn1/2*-knockout animals. *Mfrn1*$^{-/-}$/*Mfrn2*$^{-/-}$ bone marrow–derived macrophages or skin fibroblasts *in vitro* were unable to proliferate, and overexpression of Mfrn1-GFP or Mfrn2-GFP prevented this proliferation defect. Loss of both mitoferrins in hepatocytes dramatically reduced regeneration in the adult mouse liver, further supporting the notion that both mitoferrins transport iron and that their absence limits proliferative capacity of mammalian cells. We conclude that Mfrn1 and Mfrn2 contribute to mitochondrial iron homeostasis and are required for high-affinity iron import during active proliferation of mammalian cells.

Iron is essential for the formation of iron-sulfur (Fe-S) clusters and heme, both which are prosthetic groups in proteins involved in metabolic processes including redox reactions, electron transport, endoplasmic reticulum stress and oxygen transport, and DNA synthesis (DNA helicases such as XPD, polymerases, primases, ribonucleotide reductases)(1–3). The synthesis of Fe-S clusters and heme occurs in the mitochondria, therefore, iron must be imported to generate Fe-S and heme. Excess iron import into the mitochondria without efficient Fe-S cluster formation or in conditions of mitochondrial dysfunction lead to diseases including Friedreich's ataxia, X-linked and congenital sideroblastic anemias, and infantile mitochondrial complex deficiency (1–3). Two nuclear-encoded mammalian mitochondrial iron transporters, Slc25a37 (hereafter referred to as Mitoferrin1 (Mfrn1)) and Slc25a28 (hereafter referred to as Mitoferrin2 (Mfrn2)) have been implicated in iron import into mitochondria (4–8). Paralogous genes are found in all eukaryotes. Plants, *Caenorhabditis elegans*, and *Drosophila melanogaster* have only one Mfrn gene (9–12), whereas fungi and vertebrates have two Mfrns. In *Saccharomyces cerevisiae*, the Mfrn genes are named *MRS3* and *MRS4* (13, 14). *S. cerevisiae* Mrs3/Mrs4 and its plant and vertebrate homologues (Mfrn1/Mfrn2) are members of the solute carrier (SLC) family of mitochondrial transporters, which have been shown to be important in the transport of metabolites such as inorganic anions, cofactors, amino acids, and nucleotides into the mitochondrial matrix (15). Conserved functions for the homologous proteins was demonstrated by the fact that overexpression of murine *Mfrn1* rescued defects seen in the mutant zebrafish Mfrn (*frascati*) and overexpression of zebrafish *Mfrn* (*zMfrn*) complemented the poor growth on low-iron media of Δ*mrs3*Δ*mrs4* yeast cells (7). Genetic and biochemical studies have shown that Mrs3/Mrs4 are high-affinity iron importers that are only essential under iron-limiting conditions (13, 14). The vertebrate homologue Mfrn1 has been established as the iron transporter important in erythroid development and its loss is embryonic lethal with embryonic stem cells showing maturation arrest (10) and loss of *Mfrn1* in adult mice leads to severe anemia (7, 8). Deletion of *Mfrn1* in liver, heart, or muscle is not essential for development (8). Organisms with only one Mfrn such as *C. elegans*, *D. melanogaster*, and plants show

This article contains supporting information.
† Deceased.
‡ These authors contributed equally to this work.
* For correspondence: Diane M. Ward, diane.mcveyward@path.utah.edu.

lethality when deleted (9, 10). Mutations in the *D. melanogaster* homologue *dmfrn* result in male sterility, which can be rescued by providing high iron in the diet (12), suggesting other transporters can transport iron into the mitochondria under high iron conditions. It has been speculated that mammalian Mfrn2 is the mitochondrial iron importer for all other tissues, however, one study suggests that Mfrn1 and Mfrn2 are both needed in adipogenic differentiation (16).

Here, we show that Mfrn2 is not essential for viability but is important in reproduction and contributes to effective cell proliferation. $Mfrn2^{-/-}$ male mice show decreased sperm counts in seminal fluid and decreased sperm motility. $Mfrn2^{-/-}$ mice do not show reductions in mitochondrial iron levels in liver but show reduced mitochondrial manganese, cobalt, and zinc levels when animals are placed on a low-iron diet. Loss of both Mfrn1 and Mfrn2 in primary macrophages and skin fibroblasts resulted in a proliferation defect with corresponding reductions in mitochondrial oxidative phosphorylation proteins. Indeed, feeding animals a low-iron diet revealed dramatic reductions in mitochondrial iron and that loss of Mfrn1 and Mfrn2 is additive in reducing mitochondrial iron. We further show that deletion of *Mfrn1* in the liver of $Mfrn2^{-/-}$ mice significantly impairs liver regeneration.

Results

Targeting for disruption of the murine Mfrn2 (Slc25a28) gene

The murine *Mfrn2* (*Slc25a28*) gene consists of 4 exons spread over 11 kb on the reverse strand of mouse chromosome 19. We originally designed a strategy to conditionally disrupt the *Mfrn2* gene by knocking out exon 1, however, we never obtained mouse embryonic stem cell G418-resistant clones that showed the correct homologous recombination. We attributed this result to poor recombination due to the high level of repeats in the 5'-upstream region of exon 1. Mfrn2 has six predicted transmembrane domains. We hypothesized that loss of the final two transmembrane domains would disrupt function. To test this hypothesis, we generated a yeast-expressed truncated *zMfrn2* construct where the last two transmembrane domains were deleted. Although full-length *zMfrn2* complemented the loss of *Mrs3* and *Mrs4 (Δmrs3Δmrs4)*, a truncated *zMfrn2* (*truncZMfrn2*) did not complement the loss (Fig. 1*A*). To determine whether loss of the last two transmembrane domains affected protein expression or mitochondrial localization we generate mammalian constructs of full-length and truncated mouse Mfrn2 with a carboxyl GFP tag expressed under the cytomegalovirus (CMV) promoter. We transfected those constructs along with mouse Mfrn1-mCherry into mouse fibroblasts and examined expression by microscopy. Full-length Mfrn2-GFP localized with Mfrn1-mCherry, whereas, truncating the last two transmembrane domains of mouse Mfrn2 (truncMfrn2-GFP) resulted in the loss of mitochondrial localization (Fig. 1*B*). Based upon these results, we generated a "knock-out" construct that targeted deletion of exon4 in mouse *Mfrn2*, which would eliminate the last two transmembrane domains. Two Loxp sites and a neomycin-resistance gene flanked with FRT sites (FNF) were cloned on either side of exon 4 to permit excision of exon 4 (Fig. S1*A*). This construct was introduced by electroporation into mouse G4 embryonic stem (ES) cells (C57BL6/129 hybrid). ES cell clones resistant to G418 were analyzed for correct homologous recombination by Southern blotting and PCR analyses. Southern blotting analysis showed several ES clones positive for the insert (Fig. S1*B*). PCR analyses confirmed the presence of the Loxp-FRT-neomycin-FRT cassette flanking exon 4, and the second Loxp site in the recombinant *Mfrn2* locus. Cells from a single heterozygous clone (#8) were injected into C57BL/6J-derived blastocysts that were implanted into foster mothers. Chimeric animals were identified by coat color, and males were mated with C57BL/6J females to produce mice heterozygous at the *Mfrn2* locus ($Mfrn2^{floxneo/+}$). The neomycin-resistance cassette was subsequently excised by recombination of FRT sites by breeding $Mfrn2^{floxneo/+}$ mice with *flp/flp* mice that express Flp recombinase under the Rosa26 promoter generating heterozygous $Mfrn2^{flox/+}$ animals. $Mfrn2^{flox/+}$ animals were mated with CMV-Cre recombinase mice to generate $Mfrn2^{+/-}$ animals. $Mfrn2^{+/-}$ animals were mated to generate $Mfrn2^{-/-}$ animals. PCR genotyping demonstrated the generation of $Mfrn2^{+/+}$, $Mfrn2^{+/-}$, and $Mfrn2^{-/-}$ animals (Fig. 1*C*) and RT-PCR confirmed the loss of *Mfrn2* mRNA (Fig. 1*D*). $Mfrn2^{-/-}$ animals were born in the expected Mendelian ratios. Tissue-specific RT-qPCR demonstrated a 50% reduction in *Mfrn2* mRNA in heterozygotes and complete loss of *Mfrn2* mRNA in all tissues of $Mfrn2^{-/-}$ animals (Fig. 2*A*). Unfortunately, we were unable to determine Mfrn2 protein levels as available antibodies did not work in mouse tissues. There was a slight increase in liver nonheme iron levels in the absence of Mfrn2 (Fig. 2*B*) but no differences in mitochondrial nonheme iron levels as measured by the bathophenanthroline chromogen assay (Fig. 2*C*). Animals placed on a low-iron diet, however, showed changes in mitochondrial metals as assessed by inductively coupled plasma mass spectrometry (ICP-MS). Loss of Mfrn2 resulted in a slight but significant increase in total mitochondrial iron (Fe) levels and significantly decreased manganese (Mn), cobalt (Co), and zinc (Zn) with no difference in copper (Cu) levels, which was seen in both $Mfrn2^{+/-}$ and $Mfrn2^{-/-}$ liver mitochondria (Fig. 2*D*) suggesting haploinsufficiency.

We hypothesized that *Mfrn1* might be up-regulated to compensate for the loss of *Mfrn2*, however, qPCR of different organs showed no significant changes in *Mfrn1* transcript levels, with the exception of kidney where *Mfrn1* transcripts were increased 2-fold as a consequence of the loss of *Mfrn2* (Fig. 2*A*). Western blotting analysis, however, did not show an increase in kidney Mfrn1 protein levels (Fig. S2).

Loss of Mfrn2 results in decreased male fertility

$Mfrn2^{-/-}$ animals did not show any overt phenotypes in hematologic parameters (Fig. S3*A*). Breeder pairs of $Mfrn2^{-/-}$ mice revealed that the $Mfrn2^{-/-}$ males showed a decreased ability to reproduce, which worsened over time (Fig. 3*A*). The decreased fertility phenotype in mice was not fully penetrant as some $Mfrn2^{-/-}$ male mice were able to reproduce normally. The decreased male fertility could be attributed to reduced numbers of sperm (Fig. 3*B*) and significantly reduced sperm motility (Fig. 3*C*). These results confirm reports that mutations

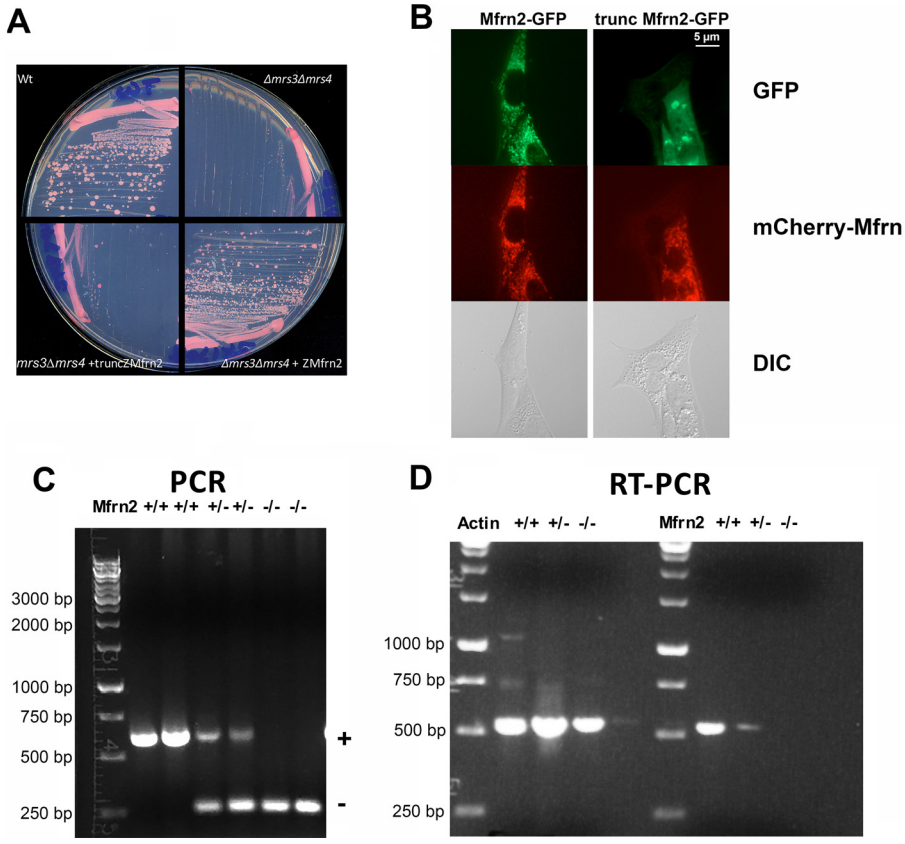

Figure 1. Strategy and generation of conditional deletion of mouse *Slc25a28 (Mfrn2)*. *A*, WT (WT) and Δ*mrs3*Δ*mrs4* cells transformed with empty vector, pZebrafish full-length Mfrn2 (zMfrn2) or pZebrafish-truncated Mfrn2 (trunZMfrn2) were grown on CM-ura bathophenanthroline sulfonate supplemented with 5 μM $FeSO_4$ for 2 days. *B*, mouse fibroblasts were transfected with plasmid containing full-length mouse Mfrn2-GFP or truncated mouse Mfrn2-GFP and Mfrn1-mCherry. Images were captured using an Olympus BX51 upright epifluorescence microscope with a ×60 oil immersion objective and QuantOne software (Olympus, Melville, NY). *C*, PCR analysis of Cre recombinase–mediated excision of exon 4 in *Slc25a28* $^{flox/flox}$ offspring. *D*, *Mfrn2* RT-PCR analysis of the offspring from the breeding of *Mfrn2*$^{+/-}$ mice using actin as a loading control.

in the *D. melanogaster dmfrn* gene result in loss of male reproduction with unorganized, small or immature sperm (12, 17).

Mfrn1 and Mfrn2 are not necessary in the adult liver

Previously, we demonstrated that liver-specific loss of Mfrn1 resulted in increased PPIX accumulation in the livers of animals fed aminolevulenic acid (ALA), a condition that bypasses the rate-limiting step in heme biosynthesis resulting in increased heme synthesis (8). We performed similar experiments in total body *Mfrn2*$^{-/-}$ mice. While feeding ALA did increase porphyrin levels in liver of all animals (note the scale), there were no statistically significant genotypic differences in PPIX levels (Fig. S3*B*). These results support that there are no differences in mitochondrial iron in the liver of *Mfrn2*$^{-/-}$ mice (if iron was decreased PPIX would accumulate) and the iron present is available and sufficient to populate PPIX when heme synthesis is increased. We did not see a significant increase in PPIX in contrast to our previous report in hepatocyte-specific *Mfrn1*$^{-/-}$ mice (8). We also did not observe the histologic changes reported previously in the hepatocyte-specific *Mfrn1*$^{-/-}$ mice. The differences with previously reported data may be due to different experimental factors such as age of the mice (6 *versus* 12 weeks) when the ALA feeding was started or a difference in the mouse environment. No changes in liver mitochondrial oxygen consumption were observed in the absence of Mfrn2 (Fig. S4*A*) supporting that mitochondrial function was not compromised.

Studies have demonstrated that Mfrn1 was necessary for red cell formation, however, Mfrn1 loss was not reported to affect heart, liver, or muscle development (8). RNA-Seq of WT mouse livers revealed that transcript levels for Mfrn1 and Mfrn2 were similar (FPKM *Mfrn1* ~705 and *Mfrn2* ~690). To determine whether the absence of both *Mfrn1* and *Mfrn2* affected liver development we generated animals with a tissue-specific deletion (hepatocyte-*Alb-Cre*) of *Mfrn1* on a *Mfrn2*$^{-/-}$ background. Surprisingly, *Alb-Cre Mfrn1*$^{f/f}$*Mfrn2*$^{-/-}$ animals were born in expected Mendelian ratios. RT-qPCR analysis of livers from 3-month–old mice demonstrated an 80% reduction in *Mfrn1* transcripts in whole liver in *Alb-Cre Mfrn1*$^{f/f}$*Mfrn2*$^{-/-}$ mice and an even greater reduction in *Mfrn1* in a crude isolation of hepatocytes confirming the ability to delete *Mfrn1* in the *Mfrn2*$^{-/-}$ background (Fig. 4*A*). Corresponding to the reduction in Mfrn1 transcripts, we observed a dramatic reduction in Mfrn1 protein. We also successfully generated hepatocyte-specific deletion of *Mfrn2* using floxed mice and these animals were born at Mendelian ratios as expected. We noted that loss of Mfrn1 or Mfrn2 in hepatocytes reduced most oxidative

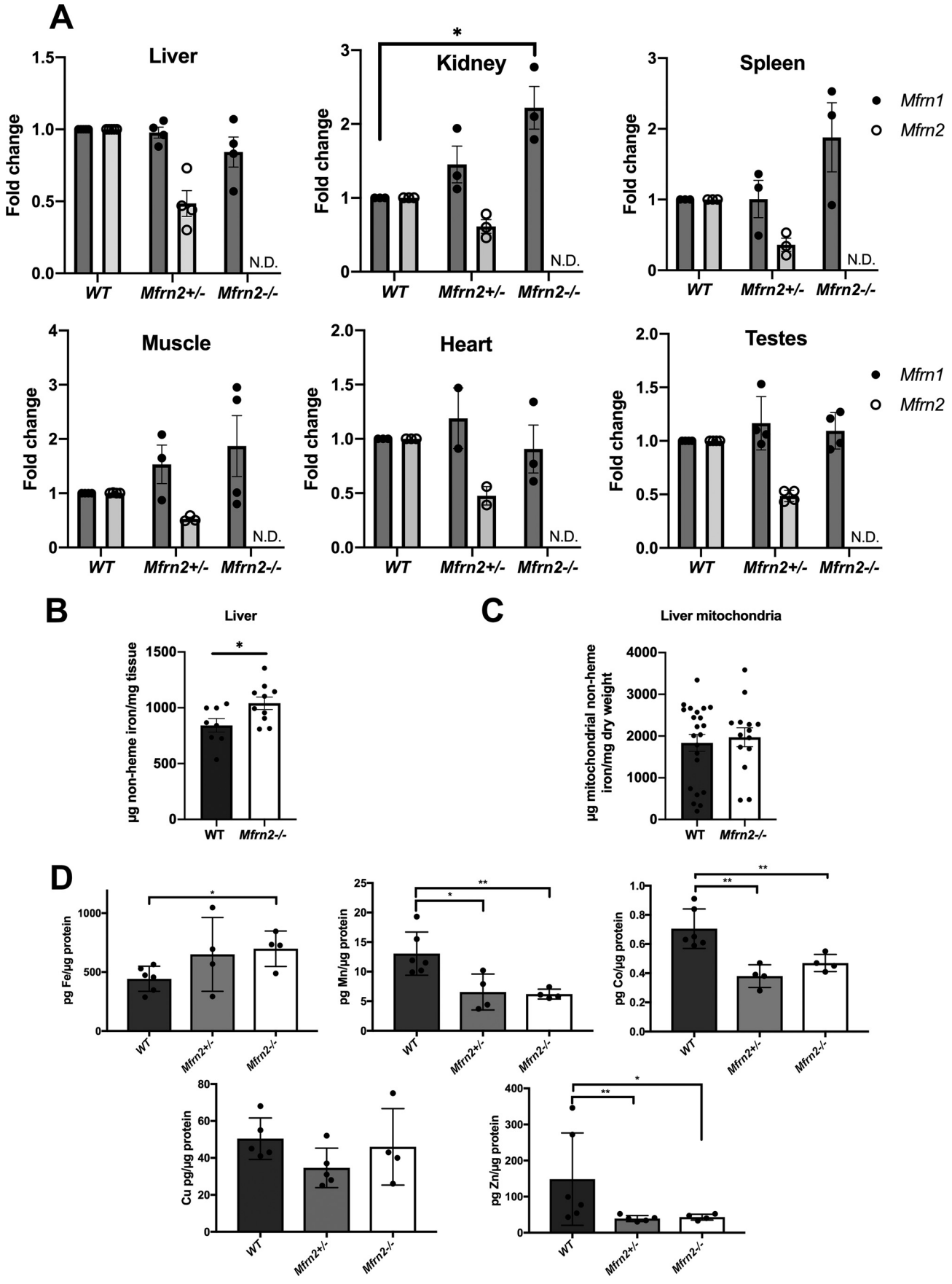
A
Liver
Kidney
Spleen
Muscle
Heart
Testes
Fold change
N.D.
WT
Mfrn2+/-
Mfrn2-/-
Mfrn1
Mfrn2
B
Liver
µg non-heme iron/mg tissue
C
Liver mitochondria
µg mitochondrial non-heme iron/mg dry weight
D
pg Fe/µg protein
pg Mn/µg protein
pg Co/µg protein
Cu pg/µg protein
pg Zn/µg protein

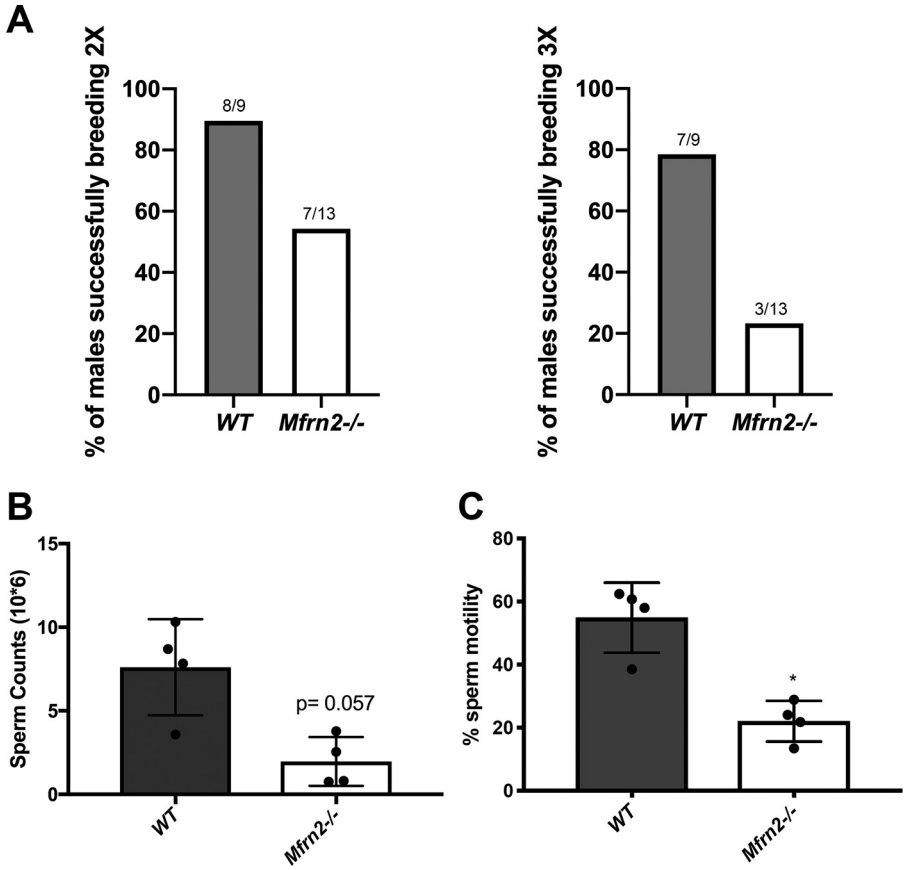

Figure 3. The absence of *Mfrn2* results in decreased male fertility. *A,* the ability to successfully breed was measured over a 3-4 month period in $Mfrn2^{+/+}$ ($n = 9$) and $Mfrn2^{-/-}$ ($n = 13$) male mice starting breeding at 2 months of age. The data are expressed as the percent of successful males breeding two (2×) or three (3×) times. *B,* sperm counts, and *C,* motility were assessed in 4-month–old $Mfrn2^{+/+}$ and $Mfrn2^{-/-}$ mice ($n = 4$). *, p value ≤ 0.05. *Error bars* represent mean ± S.E.

phosphorylation protein levels (OXPHOS) from 50 to >90% (Fig. 4*B*). Quantification revealed the most dramatic changes associated with CI-NDUFB8 protein when Mfrn1 was absent either in the single or double hepatocyte-specific knockout (Fig. 4*C*, *column 1 versus columns 2-4*). Although the decrease in protein levels was most significant when Mfrn1 was absent, CI complex activity was reduced by ~40% in all deletion strains (Fig. 4*D*). CI-NDFU8B is the first protein in the electron transport chain that catalyzes the two electron oxidation of NADH by coenzyme Q10. CII levels were also dramatically decreased in the absence of Mfrns suggesting that Fe-S cluster synthesis may be compromised. These data also suggest that both Mfrn1 and Mfrn2 contribute to iron delivery to the mitochondria for sustaining Fe-S cluster formation. Another Fe-S cluster protein whose activity is highly dependent upon the presence of the Fe-S cluster is mitochondrial aconitase. Indeed, loss of Mfrn1 or Mfrn2 reduced aconitase activity (Fig. 5*A*). Placing animals on low iron chow for 10 weeks resulted in a decrease in aconitase activity in WT animals but no statistically significant differences in aconitase activity were observed upon Mfrn1 and/or Mfrn2 hepatocyte-specific loss (Fig. 5*A*, *white bars*). We did not observe differences in the activity of the cytosolic Fe-S cluster protein xanthine oxidase (Fig. S4*B*). We also did not observe differences in the heme-containing enzyme catalase in most strains of mice fed normal chow. We did observe genotypic reductions in catalase activity when animals were placed on the low-iron diet where whole body loss of Mfrn2 showed the most dramatic reductions in catalase activity (Fig. S4*C*). These differences were not explained by changes in catalase protein levels (Fig. S4*D*).

We next examined total liver and mitochondrial iron levels in WT and hepatocyte-specific $Mfrn1^{-/-}$, $Mfrn2^{-/-}$, $Mfrn1^{-/-}Mfrn2^{-/-}$, and total body $Mfrn2^{-/-}$ mice. No statistically significant differences in liver nonheme iron levels were

Figure 2. Tissue-specific RT-qPCR in $Mfrn2^{+/+}$, $Mfrn2^{+/-}$, and $Mfrn2^{-/-}$ mice confirmed loss of *Mfrn2* mRNA in all tissues and no changes in mitochondrial iron. *A,* RT-qPCR of *Mfrn1* (*dark gray bars*), *Mfrn2* (*light gray bars*) and *actin* in liver, muscle, heart, kidney, spleen and testes using primers listed in Table 3. *Error bars* represent mean ± S.E., $n = 3$-5. *B,* livers were isolated from $Mfrn2^{+/+}$ and $Mfrn2^{-/-}$ mice. Nonheme iron was measured as described under "Materials and methods." *Error bars* represent the mean ± S.E., $n = 8$-10. *C,* mitochondria were isolated from livers of $Mfrn2^{+/+}$ and $Mfrn2^{-/-}$ mice and nonheme iron measured as described under "Materials and methods." Data are normalized to sample weight (mg). *Error bars* represent mean ± S.E., $n = 11$-19. *D,* 3-month–old animals (4-6/genotype) were fed a low-iron diet (5-6 ppm Fe/kg, Harland/Teklad) for 10 weeks and liver mitochondria were isolated. Mitochondrial metals (Fe, Mn, Co, Cu, and Zn) were detected using ICP-MS as described under "Materials and methods." $Mfrn2^{+/+}$, *dark gray bars;* $Mfrn2^{-}$, *gray bars;* and $Mfrn2^{-/-}$, *white bars*. *, p value ≤ 0.05; **, $p \leq 0.01$. *Error bars* represent the mean ± S.E.

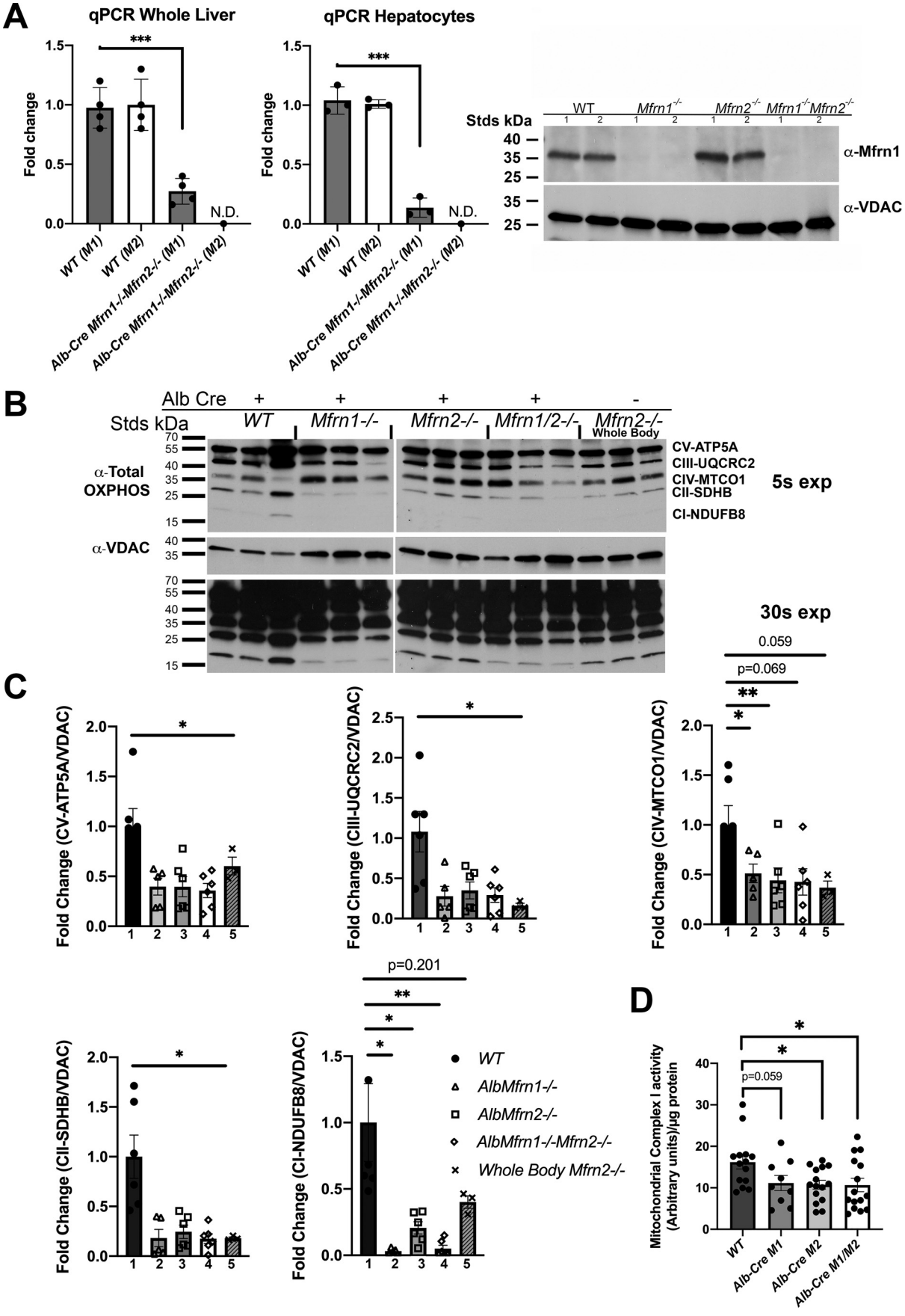
A
qPCR Whole Liver
qPCR Hepatocytes
Fold change
***
N.D.
WT (M1)
WT (M2)
Alb-Cre Mfrn1-/-Mfrn2-/- (M1)
Alb-Cre Mfrn1-/-Mfrn2-/- (M2)
Stds kDa
WT
Mfrn1-/-
Mfrn2-/-
Mfrn1-/-Mfrn2-/-
α-Mfrn1
α-VDAC
B
Alb Cre
Mfrn1-/-
Mfrn2-/-
Mfrn1/2-/-
Mfrn2-/- Whole Body
α-Total OXPHOS
CV-ATP5A
CIII-UQCRC2
CIV-MTCO1
CII-SDHB
CI-NDUFB8
5s exp
30s exp
C
Fold Change (CV-ATP5A/VDAC)
Fold Change (CIII-UQCRC2/VDAC)
Fold Change (CIV-MTCO1/VDAC)
Fold Change (CII-SDHB/VDAC)
Fold Change (CI-NDUFB8/VDAC)
p=0.201
p=0.069
0.059
WT
AlbMfrn1-/-
AlbMfrn2-/-
AlbMfrn1-/-Mfrn2-/-
Whole Body Mfrn2-/-
D
Mitochondrial Complex I activity (Arbitrary units)/µg protein
p=0.059
WT
Alb-Cre M1
Alb-Cre M2
Alb-Cre M1/M2

detected between animals fed normal chow and all animals showed reduced nonheme iron levels when placed on low iron chow (Fig. 5*B*, *blue bars*). Liver mitochondrial isolation revealed that loss of Mfrn1 (Alb-Cre*Mfrn1*$^{f/f}$ (M1)) in hepatocytes showed a trend toward reduced mitochondrial nonheme iron on normal chow, which was further decreased (approximately 50%) with loss of both Mfrn1 and Mfrn2 (Alb-Cre*Mfrn1*$^{f/f}$*Mfrn2*$^{f/f}$ (M1/M2)) even on normal chow (Fig. 5*C*, *black bars, Albcre M1/M2*). Importantly, placing animals on the low-iron diet showed significant reductions in mitochondrial nonheme iron in all animals and revealed genotype-specific differences in *Alb-CreM1, Alb-CreM2,* and *Alb-CreM1/M2* compared with WT mice (Fig. 5*C*, *blue bars*). Liver-specific loss of Mfrn2 mimicked the total body loss of Mfrn2 supporting that the mitochondrial iron changes were specific to hepatocyte loss of Mfrn2 and were not due to iron changes in other liver cell types such as Kupffer cells or fibroblasts. Furthermore, the loss of both Mfrn1 and Mfrn2 was additive resulting in the largest reduction in mitochondrial nonheme iron levels in animals fed a low iron diet (Fig. 5*C*, *blue bars, AlbcreM1/M2 low*).

To determine whether there were transcriptional changes associated with the loss of Mfrn1 and Mfrn2 in hepatocytes, we performed RNA-Seq on livers from WT and *Alb-CreMfrn1*$^{f/f}$*Mfrn2*$^{-/-}$ (*Mfrn1*$^{-/-}$*Mfrn2*$^{-/-}$) mice. A heat map of the top 100 differentially expressed genes is shown (Fig. 6*A*). *Slc25a28* (*Mfrn2*) and *Slc25a37* (*Mfrn1*) were identified in the top 50 genes with *Slc25a28* as the most dramatically changed (-3.7046 $\log_2$ ratio KO/WT) as it was a total body deletion, whereas *Slc25a37* was hepatocyte-specific deletion and the analysis was done on whole liver. Transcript changes were confirmed using RT-qPCR for a small subset of genes (Fig. S5*A*). We note that many cytochrome P450 family members transcripts were altered with eight Cyp genes in the top 40 transcripts up-regulated in *Alb-CreMfrn1*$^{f/f}$*Mfrn2*$^{-/-}$ livers representing 20% of the top up-regulated transcripts. We note that many of these enzymes are heme-containing proteins. We do not know the mechanism of up-regulation of these P450 genes but speculate that they may be up-regulated in response to liver stress. Ingenuity Pathway Analysis of the RNA-Seq data identified several pathways that were significantly affected by the absence of Mfrn1 and Mfrn2 in liver including amino acid metabolism, small molecule biochemistry, cellular movement, function and maintenance, molecular transport (Fig. 6*B, black bars*), as well as liver proliferation, inflammation, fibrosis, hepatocellular carcinoma, and hyperproliferation (Fig. 6*B, gray bars*). The most significantly ($p < 0.0001$) altered pathway was amino acid metabolism with nine genes transcript levels changed. We confirmed that amino acid metabolism was affected using LC–MS metabolomic analysis. Loss of Mfrn1 and Mfrn2 in the liver significantly changed amino acid levels, specifically tryptophan and arginine were elevated and valine, glutamine, glutamic acid, and asparagine were significantly reduced in the *Alb-CreMfrn1*$^{f/f}$*Mfrn2*$^{-/-}$ mouse livers compared with WT livers (Fig. 6*C*). In addition, AMP levels were dramatically reduced in the livers of *Mfrn1*$^{-/-}$*Mfrn2*$^{-/-}$ mice. The pathway with the most transcript level alterations was the liver hyperplasia/hyperproliferation pathway, however, we did not observe changes in liver size in the *Mfrn1*$^{-/-}$*Mfrn2*$^{-/-}$ mice compared with WT mice (Fig. S5*B*). Together, these results support that the livers of *Mfrn1*$^{-/-}$*Mfrn2*$^{-/-}$ mice are metabolically altered, which may affect cellular proliferation and differentiation (21).

Mfrn1 and Mfrn2 are necessary for in vitro cell proliferation

To determine whether Mfrn1 and Mfrn2 were necessary for cell proliferation we isolated bone marrow-derived macrophages (BMDM) from *Mfrn1*$^{f/f}$*Mfrn2*$^{+/+}$ and *Mfrn1*$^{f/f}$*Mfrn2*$^{-/-}$ mice. Dividing BMDMs were treated with recombinant Tat-Cre to excise the floxed allele and cells genotyped for deletion of the floxed allele of *Mfrn1*. RT-qPCR confirmed that we were able to delete *Mfrn1* (Fig. 7*A*). Loss of Mfrn1 but retention of Mfrn2 (*Mfrn1*$^{-/-}$*Mfrn2*$^{+/+}$ +Tat-Cre) appeared to reduce cell numbers (Fig. 7*B*, *left upper* and *lower panel* for comparison) by ~50%. Loss of Mfrn1 and Mfrn2 (*Mfrn1*$^{-/-}$*Mfrn2*$^{-/-}$) dramatically reduced cell numbers (>90%) and cells died within 72 h of Tat-Cre treatment (Fig. 7*B*, *arrowheads*). This suggests that bone marrow-derived macrophages are highly dependent upon iron transport through Mfrns for proliferation and survival in cell culture conditions. To determine whether other highly proliferative cells needed *Mfrn1* and *Mfrn2*, we generated immortalized fibroblasts from *Mfrn1*$^{f/f}$, *Mfrn2*$^{-/-}$, and *Mfrn1*$^{f/f}$*Mfrn2*$^{-/-}$ mice and exposed those cells to Tat-Cre recombinase to excise the floxed alleles of *Mfrn1* (8). We were able to successfully delete *Mfrn1* in fibroblasts as shown by genomic PCR (Fig. 7*C*, *upper band, +Tat-Cre*), however, genomic PCR revealed that the deletion was not 100% in the cell population. We predicted that deletion may be complete in some of the Tat-Cre–treated cells but incomplete in other cells, so we cloned out single cell colonies treated with Tat-Cre. We successfully generated stable *Mfrn1*$^{-/-}$ cell lines, but we were unable to clone out double null *Mfrn1*$^{-/-}$*Mfrn2*$^{-/-}$ cells (Table 1). We used the cell proliferation dye carboxyfluorescein succinimidyl ester (CFSE) to determine whether the Tat-Cre–treated fibroblasts showed reduced proliferation. Although the Tat-Cre–treated cells showed a diminution in CFSE staining, the levels remained significantly higher than control cells (Fig. 7*D*) suggesting either reduced proliferation or increased replication time.

Figure 4. Loss of hepatocyte *Mfrn1* and *Mfrn2* alters oxidative phosphorylation protein levels. *A,* RT-qPCR for *Mfrn1, Mfrn2,* and *Actin* (*control*) was performed on whole liver (*left panel*) or crude isolated hepatocytes (*right panel*). *Error bars* represent mean ± S.E., n = 3-5 mice/group. Western blots for Mfrn1 and VDAC for two animals of each genotype are shown. *B,* mitochondria were isolated from livers of 3-month–old WT (WT), *Alb-Cre Mfrn1*$^{-/-}$, *Alb-Cre Mfrn2*$^{-/-}$, *Alb-Cre Mfrn1*$^{-/-}$*Mfrn2*$^{-/-}$, and whole body *Mfrn2*$^{-/-}$ female mice. 50 μg of protein were loaded on 4–20% Tris glycine SDS-PAGE and Western blots were probed with total OXPHOS and VDAC antibodies. Representative blots with VDAC, OXPHOS 5-s and 30-s exposures are shown. n = 3/genotype/gel. *C,* bands were quantified using Fiji ImageJ and fold-change of the five OXPHOS proteins/VDAC are shown for n = 5-6 individuals animals/genotype. *Lanes 1, Alb-Cre* WT; *2, Alb-Cre Mfrn1*$^{-/-}$; *3, Alb-Cre Mfrn2*$^{-/-}$; *4, Alb-Cre Mfrn1*$^{-/-}$*Mfrn2*$^{-/-}$; *5,* whole body *Mfrn2*$^{-/-}$. *Error bars* represent mean ± S.E. *D,* mitochondrial Complex I activity was determined as described under "Materials and methods" and normalized to total protein levels. n = 9-15 animals/genotype. WT (*dark gray bar*), *Alb-Cre Mfrn1*$^{-/-}$ (*medium gray bar*), *Alb-Cre Mfrn2*$^{-/-}$ (*light gray bar*) and *Alb-Cre Mfrn1*$^{-/-}$*Mfrn2*$^{-/-}$ (*white bar*). *Error bars* represent mean ± S.E.

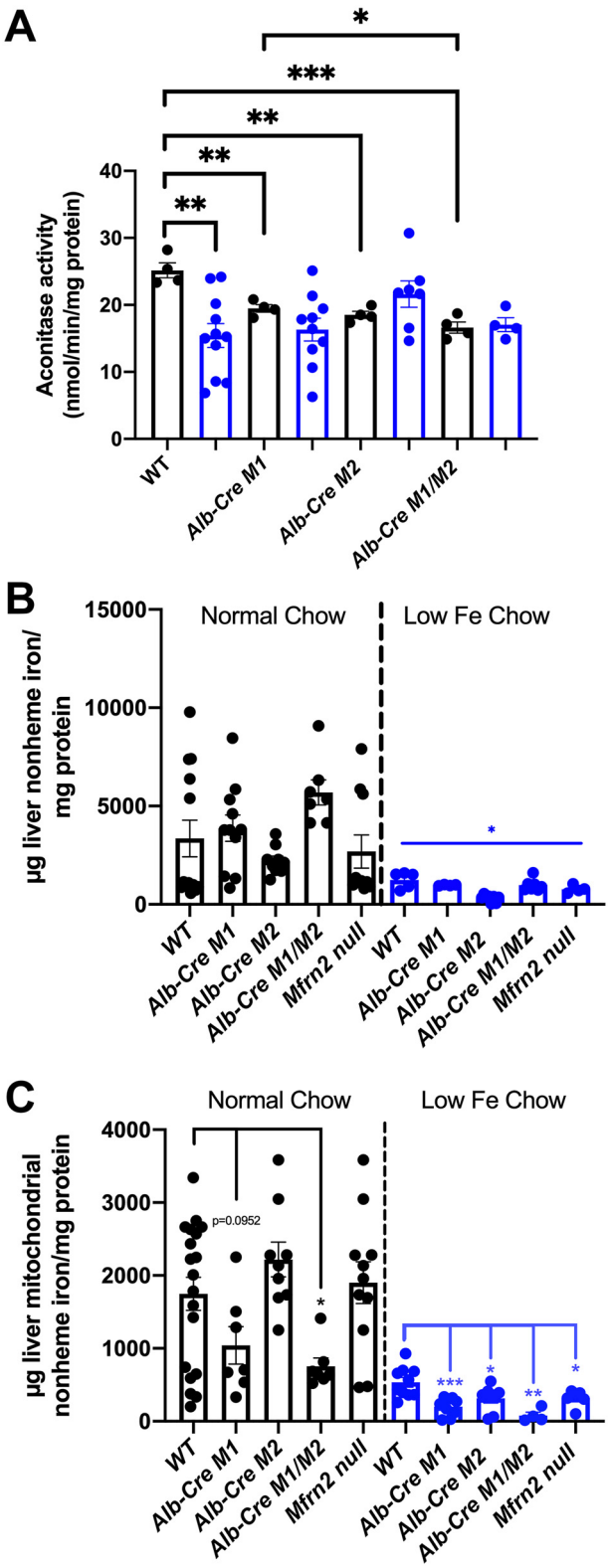

Figure 5. A low-iron diet exaggerates the changes in liver and mitochondrial nonheme iron levels seen in hepatocyte-specific loss of Mfrn1 and Mfrn2 mice. *A,* mitochondrial aconitase activity was determined from livers of 3-month–old WT (*WT*), *Alb-Cre Mfrn1*$^{-/-}$ (*M1*), *Alb-Cre Mfrn2*$^{-/-}$ (*M2*), and *Alb-Cre Mfrn1*$^{-/-}$ *Mfrn2*$^{-/-}$ (*M1/M2*) female mice fed normal (*black border bars*) or low-iron chow (*blue border bars*) for 10 weeks. n = 4-11 animals/genotype. *Error bars* represent the mean ± S.E. *B,* livers (*left panel*) and *C,* liver mitochondria (*right panel*) from mice as in *A* and total body *Mfrn2*$^{-/-}$ (*null*) mice were isolated and nonheme cellular or mitochondrial nonheme iron measured as described under "Materials and methods." Data are expressed as micrograms of liver nonheme iron/mg of protein or liver mitochondrial nonheme iron/mg of protein. n = 5-9 animals/group. *Dots* represent individual animals. *Error bars* represent the mean ± S.E. *Blue bars* represent livers of animals fed a low-iron diet for 10 weeks. *Blue bars* show statistical significance. *, $p = 0.05$ for all genotypes compared with WT low. For mitochondria, the data are expressed as micrograms of mitochondrial nonheme iron/mg of dry weight. *Error bars* represent the mean ± S.E., n = 5-18 animals/group. *Blue bars* represent liver mitochondria from animals fed a low-iron diet for 10 weeks. Student's t tests were done as described under "Materials and methods" with all compared with WT control. *, $p = 0.05$; **, $p = 0.01$; ***, $p = 0.001$.

Furthermore, Tat-Cre was not 100% efficient, therefore, we speculated that the diminution in CFSE observed may be ascribed to those cells that still retained a floxed allele of *Mfrn1* and were capable of proliferating. The Tat-Cre–treated fibroblast population (80–90% *Mfrn1*$^{-/-}$*Mfrn2*$^{-/-}$ cells) also showed significant increases in mitochondrial oxidants (Fig. 7*E*), suggesting that mitochondria are stressed due to loss of Mfrn1 in *Mfrn2*$^{-/-}$ cells. Supplementing growth media with iron (ferric ammonium citrate (FAC)) or Tf(Fe)$_2$) before and after treatment with Tat-Cre did not enhance the ability to generate proliferating *Mfrn1*$^{-/-}$*Mfrn2*$^{-/-}$ cells (Table 1). Furthermore, treatment of cells with iron-containing hinokitiol, which has been shown to promote iron transport into and within cells in the absence of membrane transporters such as Divalent Metal Transporter1 (18), before and after Tat-Cre treatment did not result in the ability to obtain *Mfrn1*$^{-/-}$*Mfrn2*$^{-/-}$ stable cell lines. To confirm that the *Mfrn1* allele could be deleted in the absence of Mfrn2, we transfected *Mfrn1*$^{f/f}$*Mfrn2*$^{-/-}$ fibroblasts with a plasmid containing mouse *Mfrn2-GFP* and then treated those cells with Tat-Cre. We successfully deleted the floxed alleles of *Mfrn1* with ~85% efficiency. We sorted for single GFP-positive cells, cloned out those cells, confirmed deletion of the floxed alleles of *Mfrn1* and that those clones that showed loss of *Mfrn1* but retention of the *Mfrn2-GFP* plasmid remained viable and capable of proliferating. Similar results were obtained if we transfected cells with a plasmid containing *Mfrn1-GFP* (data not shown). Importantly, *Mfrn1*$^{-/-}$*Mfrn2*$^{-/-}$ *pMfrn2-GFP* cells were unable to lose the *pMfrn2-GFP* when antibiotic selection was removed, whereas *Mfrn1*$^{-/-}$ *Mfrn2*$^{+/+}$ cells containing *pMfrn2-GFP* were able to lose the plasmid when selection was removed (Fig. 7*F*). These results demonstrate that both Mfrn1 and Mfrn2 are necessary for fibroblast proliferation. Attempts to measure changes in mitochondrial iron levels in the Tat-Cre cell culture experiments were unsuccessful using either fluorescent dyes or ICP-MS (data not shown). We do not know why the mitochondrial fluorescent dyes (RPA or MitoFerroGreen) did not work. We believe that the inability to use ICP-MS was due to the limited amounts of mitochondria we were able to obtain from cells after Tat-Cre treatment. Together, these data show that other mitochondrial metal transporters are sufficient for the majority of heme and Fe-S cluster synthesis but they cannot compensate for the loss of Mfrns during increased proliferation demand.

To identify consequences of loss of *Mfrn1* and *Mfrn2* that might lead to an inability to proliferate, we generated a *Mfrn1*$^{-/-}$*Mfrn2*$^{-/-}$ fibroblast cell line that harbored a *TET*-regulated human *MFRN1-GFP* expression vector, which was turned off in the presence of doxycycline (Fig. 8*A*). We noted that some cells expressed higher levels of Mfrn1-GFP

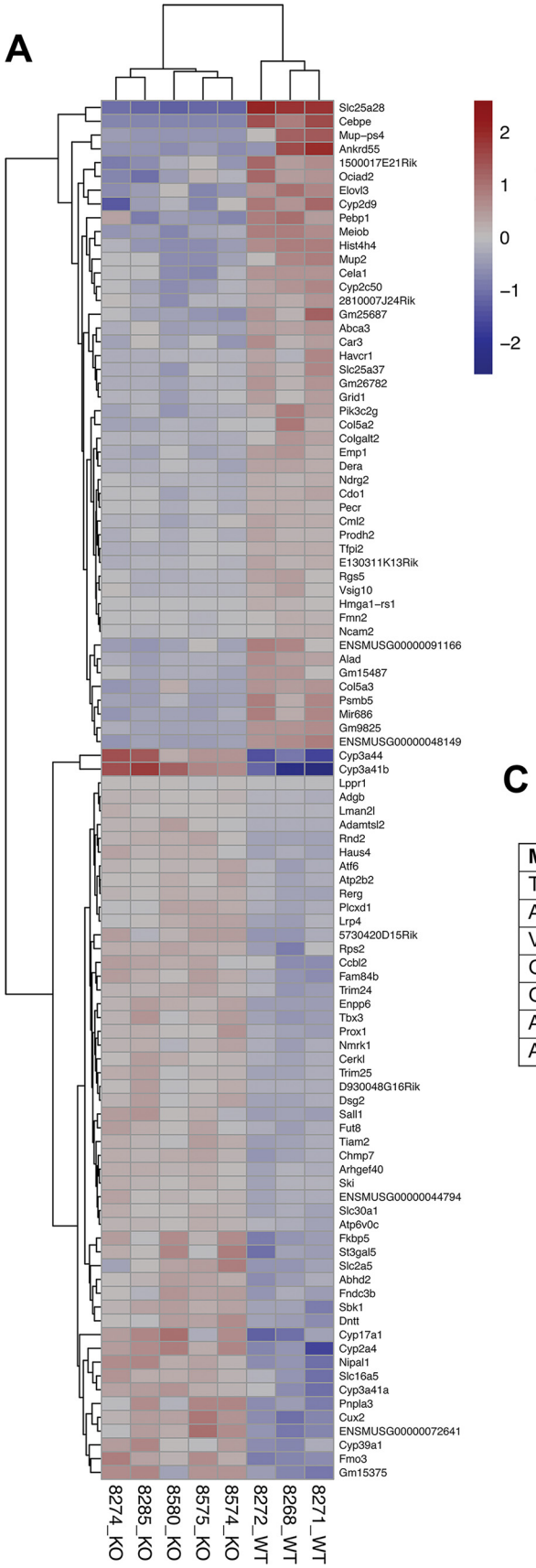

C

Metabolite	Double null/WT	log2(FC)	raw.pval	-log10(p)
Tryptophan	3.4624	1.7918	0.02566	1.5907
Arginine	1.7197	0.78215	0.00056343	3.2492
Valine	0.6008	-0.73503	0.012183	1.9142
Glutamine	0.23076	-2.1155	0.0099085	2.004
Glutamic acid	0.18728	-2.4168	0.011872	1.9255
Asparagine	0.097061	-3.365	0.0010769	2.9678
AMP	0.08248	-3.5998	0.0050106	2.3001

compared with others. We generated clonal population of these cells and the analyses were done on two separate clones. Images were quantified for Mfrn1-GFP fluorescence and we noted that expression of Mfrn1-GFP was long lived with some protein still detected even after 96 h growth in doxycycline (Fig. 8*B*). This may reflect expression under the tetracycline promoter or that the $t_{1/2}$ of Mfrn1 is long. Previous studies have suggested that mitochondrial inner membrane proteins have a $t_{1/2}$ of ~36 h (19). We isolated mitochondria from the two clones (1 and 2) incubated in the presence or absence doxycycline and examined the levels of Mfrn1-GFP, mitochondrial VDAC, and oxidative phosphorylation proteins by Western blotting. As expected, Mfrn1-GFP was dramatically reduced in cells grown in doxycycline (Fig. 8, *C* and *D*). Decreases in Mfrn1-GFP levels in *Mfrn1*$^{-/-}$*Mfrn2*$^{-/-}$ fibroblasts resulted in significant reductions in OXPHOS complex protein levels (Fig. 8*E*, *+Dox*). The change in OXPHOS complex proteins was specific to loss of hMfrn1-GFP and was not the result of doxycycline toxicity as in *Mfrn1*$^{f/f}$ *Mfrn2*$^{-/-}$ we did not observe changes in GAPDH (a cytosolic marker) or reductions in VDAC (a mitochondrial marker) upon exposure to doxycycline (Fig. 8*C*, *Con – versus + Dox*). These results support that a consequence of loss of Mfrns is reduced levels of mitochondrial oxidative phosphorylation proteins, most dramatically those containing Fe-S clusters such as CIII and CII. We note that addition of doxycycline induced a slight decrease in complex II of the OXPHOS proteins in control cells compared with control cells without Dox. Previous studies have suggested that tetracyclines can disturb mitochondrial function (20), however, the decrease was only seen in CII and was much more dramatic in the "shut-off" system further underscoring that the reduction/loss of Mfrn1-GFP contributes to reduced OXPHOS proteins.

Mfrn1 and Mfrn2 are necessary for liver regeneration

To determine whether the mitochondrial oxidative phosphorylation changes and metabolic changes implicated in the RNA-Seq and metabolomic results affected proliferation, we took advantage of the fact that the liver can regenerate *in vivo* after tissue loss (21). We performed 2/3 partial hepatectomies on 3-month–old WT*Alb-Cre*, *Alb-Cre Mfrn1*$^{f/f}$*Mfrn2*$^{+/+}$, *Alb-Cre Mfrn1*$^{+/+}$*Mfrn2*$^{-/-}$, and Alb-Cre *Mfrn1*$^{f/f}$*Mfrn2*$^{-/-}$ mice. We examined cell proliferation pre- and post-hepatectomy using the cell proliferation marker Ki67 (22). Histologic examination of liver samples at the time of hepatectomy showed minimal Ki67 staining in all genotypes (Fig. 9*A*, *pre*). Forty-eight hours post-hepatectomy, WT *Alb-Cre* and *Alb-Cre Mfrn1*$^{+/+}$ *Mfrn2*$^{-/-}$ liver samples showed increased Ki67 staining, whereas, both Alb-Cre *Mfrn1*$^{f/f}$ and Alb-Cre *Mfrn1*$^{f/f}$*Mfrn2*$^{-/-}$ livers showed decreased Ki67 staining compared with WT (Fig. 9*A*, *post*). Quantification of the Ki67 staining revealed a trend toward decreased Ki67 staining in *Alb-Cre Mfrn1*$^{f/f}$*Mfrn2*$^{+/+}$ animals that was reduced further when both Mfrns were lost (Fig. 9*B*). We noted some evidence of steatosis in histologic analysis predominantly in the livers after partial hepatectomy (WT 3/7, Alb-Cre *Mfrn1*$^{f/f}$ 3/8, *Alb-Cre Mfrn1*$^{+/+}$*Mfrn2*$^{-/-}$ 2/7, and Alb-Cre *Mfrn1*$^{f/f}$*Mfrn2*$^{-/-}$ 6/9) with the Alb-Cre *Mfrn1*$^{f/f}$*Mfrn2*$^{-/-}$ livers showing the highest incidence (66.7%). This suggest that liver lipid metabolism under the stress of regeneration is compromised by the loss of Mfrn1 and Mfrn2. Our previous RNA-Seq (Fig. 5*C*) revealed dramatic reductions in both *Cebpe* and *Hist4h4* transcripts in *Alb-CreMfrn1*$^{f/f}$ *Mfrn2*$^{-/-}$ livers compared with WT livers (Fig. 9, *C* and *D*), whereas other Cebp and histone family members did not show significant changes in transcript levels. We were unable to detect these proteins using conventional Western blots (data not shown). Cebpe is a member of the CCAAT enhancer-binding protein family of transcription factors that regulate the expression of genes involved in mitotic expansion and a role for Cebpe has been shown for granulocyte differentiation (23–25) as well as in acute lymphoblastic leukemia proliferation (26). One target gene of the Cebp family, specifically Cebpb, is *Hist4h4*, which contains Cebp-binding sites in its promoter region and is activated during mitotic clonal expansion (27). *Hist4h4* encodes for histone H4, which is important in nucleosome structure and increased expression is associated with some types of highly proliferative cancer (28). It may be that in the absence of Cebpe in hepatocytes, *Hist4h4* does not get activated and thus limits mitotic expansion. Together with our metabolomic results that show significant reductions in essential amino acids and the loss of *Cebpe* expression and reduced *Hist4h4* transcripts could be contributing to reduced proliferative capacity in *Alb-CreMfrn1*$^{f/f}$*Mfrn2*$^{-/-}$ livers.

Discussion

Mitoferrins have been identified in all eukaryotes (7, 10, 12–14, 29). Mfrn1 is essential and is necessary for red cell development (7, 8). In contrast, very little is known about Mfrn2 and its role in mitochondrial iron homeostasis (4, 6, 16). In our current study, we determined that total body loss of Mfrn2 did not affect viability and showed no overt phenotypes. However, when combined with deletion of Mfrn1 in the liver, it resulted in reduced mitochondrial iron and reduced OXPHOS proteins including Fe-S cluster proteins CI-NDUF8B and CII-SDHB. Loss of Mfrn1 and Mfrn2 also resulted in a dramatic reduction in liver regeneration capacity. We also showed that primary and immortalized cells lost proliferative capacity in the absence of Mfrn1 and Mfrn2. Previous studies have shown that altering OXPHOS protein activity affects cell amino acid levels and proliferation (30, 31). Our RNA-Seq data suggested that there are significant transcriptional shifts in the liver in response to loss of both Mfrns with the most significant changes in amino acid metabolism. Furthermore, we determined that several amino

Figure 6. Loss of Mfrn1 and Mfrn2 results in significant transcriptional and metabolic changes in the liver. *A,* RNA-Seq was performed on three WT and five Alb-Cre *Mfrn1*$^{-/-}$*Mfrn2*$^{-/-}$ (DKO) mouse livers. A heat map showing gene expression differences in 100 protein-coding genes 3 WT and 5 Alb-Cre *Mfrn1*$^{-/-}$*Mfrn2*$^{-/-}$ animals is provided. *B,* Ingenuity Pathway Analysis (Qiagen) of RNA-Seq results from *A* showing the number of genes significantly changed in particular pathways in Alb-Cre *Mfrn1*$^{-/-}$*Mfrn2*$^{-/-}$ compared with WT for cellular function and metabolism (*black bars*) and hepatotoxicity (*gray bars*) and the corresponding *p* values for those gene pathway changes. *C,* liver metabolomics was performed on four WT and four Alb-Cre *Mfrn1*$^{-/-}$*Mfrn2*$^{-/-}$ mouse livers. LC–MS and statistical analyses were done as described under "Materials and methods." Specific amino acid changes are shown. The data are presented as the fold-change Alb-Cre *Mfrn1*$^{-/-}$*Mfrn2*$^{-/-}$ *versus* WT.

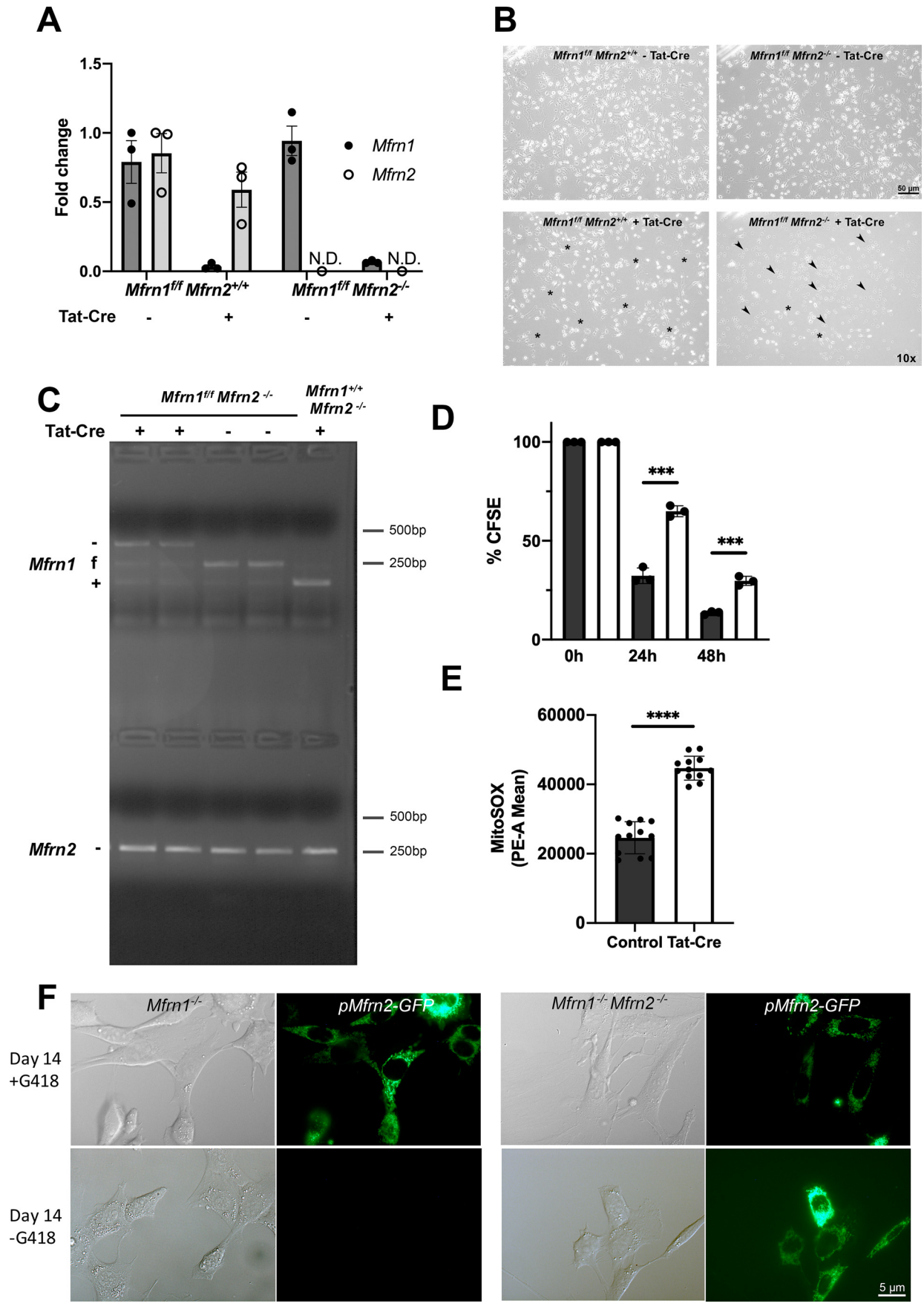
A
Fold change
1.5
1.0
0.5
0.0
Mfrn1
Mfrn2
N.D.
N.D.
Mfrn1f/f Mfrn2+/+
Mfrn1f/f Mfrn2-/-
Tat-Cre - + - +
B
Mfrn1f/f Mfrn2+/+ - Tat-Cre
Mfrn1f/f Mfrn2-/- - Tat-Cre
50 µm
Mfrn1f/f Mfrn2+/+ + Tat-Cre
Mfrn1f/f Mfrn2-/- + Tat-Cre
10x
C
Mfrn1f/f Mfrn2 -/-
Mfrn1+/+ Mfrn2 -/-
Tat-Cre + + - - +
Mfrn1 - f +
500bp
250bp
Mfrn2 -
500bp
250bp
D
% CFSE
100
50
0
***
***
0h
24h
48h
E
MitoSOX (PE-A Mean)
60000
40000
20000
0
****
Control Tat-Cre
F
Mfrn1-/-
pMfrn2-GFP
Mfrn1-/- Mfrn2-/-
pMfrn2-GFP
Day 14 +G418
Day 14 -G418
5 µm

Table 1

Percentage of clones showing *Mfrn1*$^{-/-}$ genotype after Tat-Cre

Mfrn1$^{f/f}$, *Mfrn*$^{f/f}$*Mfrn2*$^{-/-}$, *Mfrn1*$^{f/f}$*pMfrn2-GFP*, or *Mfrn*$^{f/f}$*Mfrn2*$^{-/-}$*pMfrn2-GFP* cells incubated for 48 h with or without ferric ammonium citrate (FAC), Tf(Fe)$_2$, or Fe-hinokitiol were treated with recombinant Tat-Cre as described under "Materials and methods" and single cell colonies cloned out. DNA was isolated from clones and PCR genotyping performed using primers listed in Table 2. Clones isolated from the Tat-Cre–treated *Mfrn1*$^{f/f}$ *Mfrn2*$^{-/-}$ were genotypically either *Mfrn1*$^{f/f}$*Mfrn2*$^{-/-}$ or *Mfrn1*$^{f/-}$*Mfrn2*$^{-/-}$. No stable double null cells were observed.

Pre-Tat-Cre fibroblast genotype	Post-Tat-Cre	Percentage	Number of clones
Mfrn1$^{f/f}$	*Mfrn1*$^{-/-}$	43.1%	9/20
Mfrn1$^{f/f}$*pMfrn2-GFP*	*Mfrn1*$^{-/-}$	50.0%	5/10
Mfrn1$^{f/f}$*Mfrn2*$^{-/-}$	*Mfrn1*$^{-/-}$*Mfrn2*$^{-/-}$	00.0%	0/100
Mfrn1$^{f/f}$ *Mfrn2*$^{-/-}$pMfrn2-GFP	*Mfrn1*$^{-/-}$*Mfrn2*$^{-/-}$	87.0%	47/54
10 μM FAC *Mfrn1*$^{f/f}$ Mfrn2$^{-/-}$	*Mfrn1*$^{-/-}$*Mfrn2*$^{-/-}$	00.0%	0/26
10 nM Tf(Fe)$_2$ *Mfrn1*$^{f/f}$ *Mfrn2*$^{-/-}$	*Mfrn1*$^{-/-}$*Mfrn2*$^{-/-}$	00.0%	0/15
2 μM Fe-hinokitiol *Mfrn1*$^{f/f}$ *Mfrn2*$^{-/-}$	*Mfrn1*$^{-/-}$*Mfrn2*$^{-/-}$	00.0%	0/63

acid levels were significantly altered in the Mfrn1/2 null livers with asparagine, glutamine, glutamic acid, and valine dramatically reduced. Mammals cannot synthesize all the amino acids necessary for protein synthesis/biomass accumulation and cell proliferation and rely heavily on glutamine, which can be converted to several other amino acids including proline, aspartate, and asparagine (for review, see Zhang *et al.* (32)). We speculate that the diminution in mitochondrial function results in diminished glutamine levels, which results in other amino acid limitations and the consequence of an inability to proliferate. Our results provide a possible mechanistic explanation for the loss of proliferative capacity when Mfrns are absent.

Our RNA-Seq data also highlight the fact that transcripts for the CCAAT/transcription factor family member Cebpe as well as Hist4H4 are dramatically reduced in the Mfrn1/2 null livers. A role for Cebpe in liver homeostasis/proliferation has not been demonstrated before but a role for Cebpe in mitotic expansion has been shown (26). Indeed, Studd and colleagues (26) have shown the Cebpe binds to the promoters of electron transport and energy generation genes and its depletion reduces cell growth in leukemia. Our data suggest that this may be true for hepatocytes too. RNA-Seq also revealed that *Hist4H4* transcripts were dramatically decreased in the Mfrn1/2 DKO livers. Histone expression is cell cycle regulated to ensure accumulation of histones during DNA replication to protect chromatin (28). Furthermore, studies in yeast have shown partial depletion of histone H4 increases homologous recombination and genetic instability (33). That the levels of H4 are reduced >3-fold in the livers of Mfrn1/2 null mice provides another possible mechanism to explain why cell proliferation is dramatically reduced in both primary and immortalized cells.

Our results also show that male fertility is affected by the loss of Mfrn2 with decreased sperm numbers and sperm motility although the phenotype was not fully penetrant. We hypothesize that this may be due to the presence of Mfrn1. Our results in cell proliferation demonstrate that there is an additive effect to the loss of Mfrn1 and Mfrn2 and that these proteins both transport iron into mitochondria. We anticipate that the loss of Mfrn1 would also affect male fertility, however, further investigation into the role of Mfrn1 in male fertility is beyond the scope of this study. It may also be that Mfrn2 is the predominant mitochondrial iron transporter in testes and Mfrn1 does not play a role but that iron can be imported through other low-affinity divalent metal transporters. One prediction of this would be a diminution in other mitochondrial metals due to iron competition, which was seen in livers of low iron-fed mice in response to loss of Mfrn2. We did not measure mitochondrial metal levels in testes due to limited reagents, however, if this were found to be the case in testes then one could conclude that Mfrn2 is the homologue of dMfrn, as mutations in *dMfrn* result in male infertility in *D. melanogaster* (17).

Loss of Mfrn2 alone did not affect mitochondria nonheme iron levels in animals fed normal chow, however, when animals were placed on low-iron chow total mitochondrial iron (Fe and heme-Fe) was slightly increased in *Mfrn2*$^{-/-}$ mouse livers, whereas, mitochondrial cobalt (Co), manganese (Mn), and zinc (Zn) levels were reduced. This suggests that either Mfrn2 transports these metals and does not transport Fe or the loss of Mfrn2 drives Fe import through other mitochondrial metal transporters at the consequence of reduced Co, Mn, and Zn. We speculate that the essential nature of mitochondrial iron would provide the demand to alter metal transport specificity. We did not see significant changes in Cu levels supporting that

Figure 7. Mfrn1 and Mfrn2 are necessary for cell proliferation. *A,* bone marrow-derived macrophages were isolated from *Mfrn1*$^{f/f}$*Mfrn2*$^{+/+}$ and *Mfrn1*$^{f/f}$ *Mfrn2*$^{-/-}$ mice, cells were cultured as described previously until actively proliferating (48), treated with or without recombinant Tat-Cre, and 48 h post-Tat-Cre treatment deletion of the floxed *Mfrn1* allele was confirmed by RT-qPCR using the primers with β-actin primers as control (Table 3). *Error bars* represent mean ± S.E., $n = 3$. *B,* cells as in *A* were examined by microscopy 72 h post-Tat-Cre treatment. Representative whole fields are shown. Whole field images were captured with an Olympus tissue culture microscope with a ×10 objective. Rounded luminescent Tat-Cre cells represent actively dividing cells and are noted by an *asterisk* (*). *Arrowheads* represent regions of cell death. *C,* skin fibroblasts isolated and immortalized from 3-month–old *Mfrn2*$^{-/-}$ and *Mfrn1*$^{f/f}$*Mfrn2*$^{-/-}$ mice were treated with or without recombinant Tat-Cre and 48 h post-treatment genomic DNA was harvested and PCR for *Mfrn1* and *Mfrn2* performed using the primers described in Table 2. (+) WT *Mfrn1* allele; (*f*) floxed *Mfrn1* allele; and (−) *Mfrn1* null allele and *Mfrn2* background was always null (−). *D,* cells as in *C* were labeled with CFSE at time 0 and CFSE levels in the cell populations after 24 and 48 h quantified using flow cytometry. *Black bars,* −Tat-Cre; *white bars,* +Tat-Cre. The data are expressed as the percentage of time 0 CFSE for 2-3 × 10^4 cells ($n = 3$). *Error bars* represent mean ± S.E. ***, $p < 0.0003$ compared with the control at 24 or 48 h. *E,* mitochondrial oxidants were measured by flow cytometry using MitoSOX in *Mfrn1*$^{f/f}$*Mfrn2*$^{-/-}$ cells treated without (*Control*) or with Tat-Cre. The data are expressed as the mean fluorescence with 1-3 × 10^4 cells per sample ($n = 12$ replicates). *Error bars* represent mean ± S.E. ****, $p < 0.0001$. *F, Mfrn1*$^{f/f}$ and *Mfrn1*$^{f/f}$*Mfrn2*$^{-/-}$ cells were transfected with a CMV-based plasmid containing Mfrn2-GFP or Mfrn1-GFP (data not shown) and cells grown in G418 to maintain the plasmid. Cells were then treated with Tat-Cre as in *A*, deletion of the floxed *Mfrn1* allele was confirmed and cells split onto glass coverslips and grown in DMEM with or without G418 selection for 14 days. Images were captured using an Olympus BX51 upright epifluorescence microscope with a ×60 oil immersion objective and QuantOne software (Olympus, Melville, NY). Representative fields are shown. $n = 10$-20 fields/group.

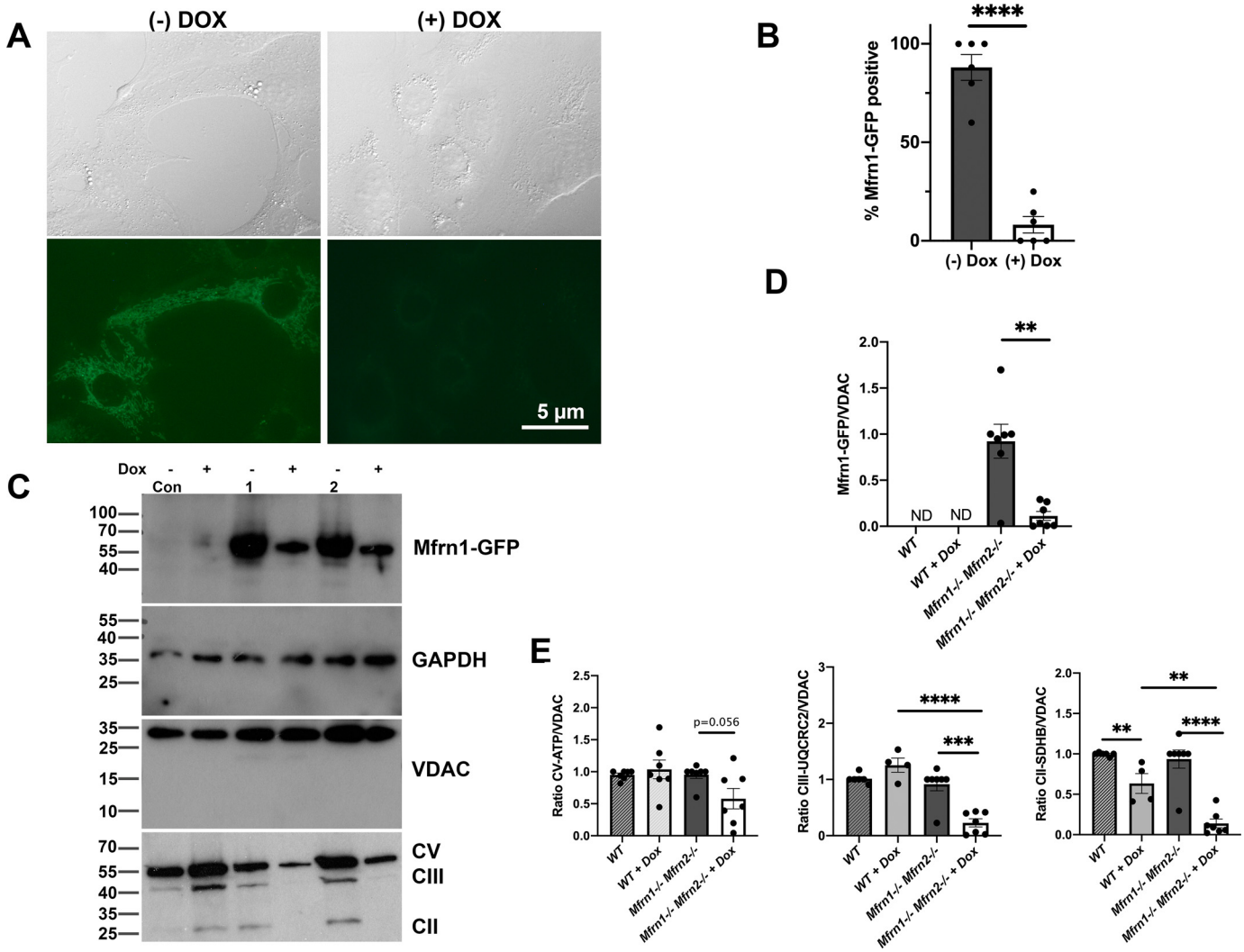

Figure 8. Loss of Mfrn1 and Mfrn2 results in decreased mitochondrial oxidative phosphorylation proteins. *A, Mfrn1*$^{-/-}$*Mfrn2*$^{-/-}$ LV-TetOff and pLV-Tight.HuMFRN1-GFP clone #44, fibroblasts were grown in the absence or presence of 2 μg/ml of doxycycline for 96 h and imaged as described under "Materials and methods." *B,* quantification of *A* where the % of cells positive for Mfrn1-GFP was determined from 20 fields with 4-8 cells/field. *Error bars* represent the mean ± S.E. *C, Mfrn1*$^{-/-}$*Mfrn2*$^{-/-}$ LV-TetOff pLV-Tight.HuMFRN1-GFP clone 1, clone 2, and *Mfrn1*$^{f/f}$*Mfrn2*$^{-/-}$ fibroblast (Con) were harvested, whole cells and mitochondria were isolated. BCA protein determinations were performed and 50 μg of whole cell lysate or mitochondrial lysate with Laemmli buffer was heated to 65 °C for 20 min. Samples (mitochondria or cytosol) were run on 4–20% Tris glycine SDS-PAGE and Western blotted for GFP, GAPDH, VDAC, or mixture OXPHOS proteins. A representative blot is shown. *D,* the ratio of Mfrn1-GFP levels compared with VDAC levels in the blot were determined using Fiji ImageJ software; *n* = 4. *E,* the ratio of OXPHOS proteins CV, CIII, and CII compared with VDAC levels were determined as in *D*. *Error bars* represent the mean ± S.E.

Cu is also essential and would not be outcompeted by Fe in the absence of Mfrn2. Divalent metal transporters have been shown to have different affinities for several metals. Recent studies using an *in vitro* system have shown that Mfrn1 transports Fe^{2+} as well as Mn, Co, Zn, and Cu (34). Metal specificity for Mfrn2 has not yet been determined. It may be that in the absence of Mfrn2, Mfrn1 increases Fe transport at the consequence of other metal import. *In vitro* reconstitution assays are necessary to distinguish between these possibilities. Our liver *Mfrn1*$^{-/-}$*Mfrn2*$^{-/-}$ mitochondrial iron measurements support that Mfrn1 and Mfrn2 transport iron as their loss is additive to the reduction in mitochondrial iron observed.

We were extremely surprised to find viable animals when *Mfrn1* was deleted in the livers of whole body *Mfrn2*$^{-/-}$ mice. We anticipated that animals would not be viable due to the essential nature of iron import into mitochondria for heme and Fe-S cluster formation. Hepatic stipulation during development occurs at day e8.5 to e9.0 and albumin is expressed at this time in the liver bud (35, 36), suggesting that deletion of *Mfrn1* should occur before birth. We did not, however, examine *Mfrn* mRNA in the developing fetus. Our RT-qPCR and Western blotting results showed loss of *Mfrn1* mRNA and protein in 3-month–old mice. Studies by Hopkinson and colleagues (37) suggest that during *in vitro* stem cell to hepatic lineage differentiation, hepatic progenitor cells are primarily dependent upon glycolysis and hepatic maturation depends on mitochondrial respiration, but that both stages of development show some oxidative phosphorylation. Our results support that hepatic lineage is not compromised due to loss of Mfrns, but both Mfrns are necessary when the demand for mitochondrial respiration is increased (*e.g.* regeneration). Our *in vitro* cell culture systems

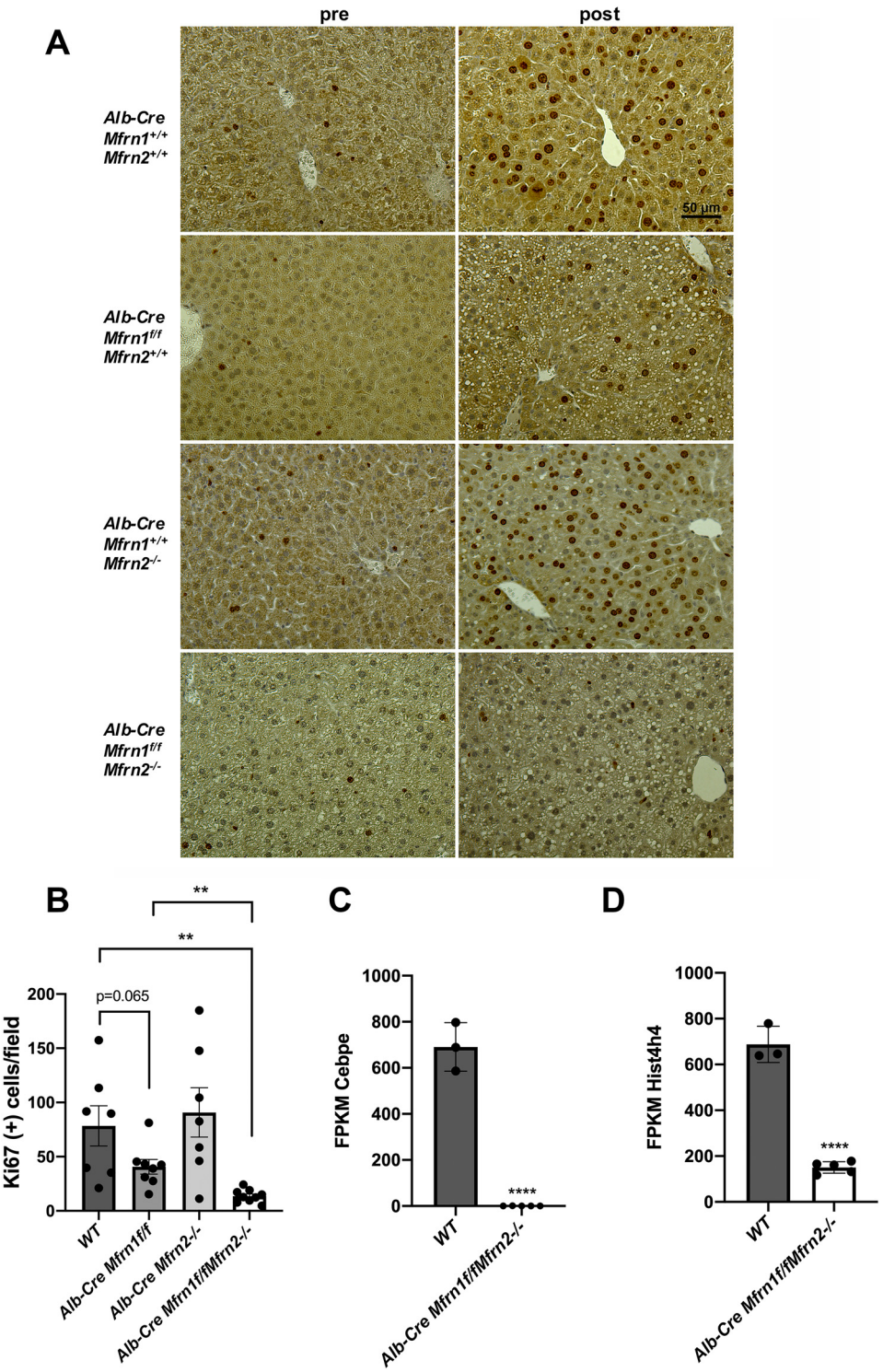

Figure 9. Mfrn1 and Mfrn2 are necessary for liver regeneration. *A,* two-thirds partial hepatectomy were performed on 3-month–old WT (*WT*), *Alb-Cre Mfrn1$^{f/f}$*, *Mfrn2$^{-/-}$*, and *Alb-Cre Mfrn1$^{f/f}$Mfrn2$^{-/-}$* female mice. Liver sections were fixed in formalin and processed for Ki67 staining immediately after hepatectomy (pre) and 48 h post-hepatectomy as described under "Materials and methods." Images were captured using an Olympus BX51 upright microscope and QuantOne software (Olympus, Melville, NY) with a ×20 objective and five fields capture per liver. Representative images are shown. *B,* quantification of Ki67 staining (n = 7-9 animals/genotype with ~200-250 cells/field/five fields) were performed on slides coded by animal ear tag numbers and genotypes were not revealed until after quantification. Student's t tests were performed and p values were determined compared with the WT (*Alb-Cre Mfrn1$^{+/+}$Mfrn2$^{+/+}$*) Ki67 staining. *C, Cebpe* and *D, Hist4h4* RNA sequencing reads/transcripts (FPKM) from WT and *Alb-Cre Mfrn1$^{f/f}$Mfrn2$^{-/-}$* female mice (Fig. 6*A*). ****, $p < 0.0001$ by Student's t test.

support this conclusion as knockout cells can be generated but loss of both Mfrn1 and Mfrn2 results in an inability to proliferate. We observed that the *in vitro* loss of proliferative capacity could not be corrected by the addition of exogenous iron (Tf $(Fe)_2$) or ferric/ferrous iron nor the iron-binding molecule hinokitiol (18). This suggests that simply increasing cellular

iron is not sufficient, but that mitochondrial iron transport through Mfrns is necessary during cell proliferation.

The results of the low-iron diet suggest that Mfrns are more important for iron transport under iron-limited conditions. This is also true in yeast where loss of Mrs3 and Mrs4 does not result in a phenotype until cells are grown under low-iron conditions (13, 14, 38). It is interesting to speculate regarding transporters that might compensate for the loss of Mfrns. Candidates suggested from the literature include the mitochondrial calcium uniporter MCU1 (39–41) and pyrimidine transporters Slc25a33 and Slc25a36 (mammalian Rim2 homologues) (42–44). It is also possible that there are other unidentified transporters that can transport Fe under the stress conditions provided by the loss of Mfrns. Further studies are needed to identify other transporters or mechanisms that provide iron during liver development. In conclusion, this study demonstrates that both Mfrns contribute to mitochondrial iron homeostasis and that when proliferation is increased both Mfrn1 and Mfrn2 high-affinity iron transport is necessary.

Materials and methods

Generation of the Slc25a28 targeting vector

To generate the *Slc25a28*-floxed mouse, exon 4 of mouse *Slc25a28* was floxed using standard BAC recombineering techniques in SW106 *Escherichia coli* cells. C57BL/6 mouse BAC DNA clone (RP23-181M12) was obtained from BACPAC Resources (RRID:SCR_001520) (Oakland, CA) and a Loxp-Neo-Loxp (LNL) cassette was introduced 250 bp upstream of the exon 4 followed by Cre-based recombination resulting in a single Loxp sequence. Next, a Frt-Neo-Frt-Loxp (FNFL) cassette was introduced into the 3'-UTR within exon 4 (339 bp downstream of the stop codon). The targeting construct was then completed by a homologous recombination-based retrieval procedure using a diphtheria toxin A (DTA)-Amp^r cassette to include a short arm (2582 bp) at the upstream of the single Loxp and a long arm (4430 bp) at the downstream of the FNFL cassette, respectively. The construct was authenticated by activating Cre recombinase and by DNA sequencing.

Screening of the ES cell clone and genotyping of animals

ES cell clones resistant to G418 and ganciclovir were analyzed for correct homologous recombination by Southern blotting and PCR analyses. For Southern blotting analysis, DNA was purified, digested by SpeI, and probed with a 5'-flanking probe generated as a PCR product using the forward primers M2probeF1 or M2probeF2 and the reverse primers M2probeR1 or M2probeR2 (Table 2). Cells from a single heterozygous clone (Np. 8) were injected into C57BL/6J-derived blastocysts that were implanted into foster mothers. Chimeric animals were identified by coat color, and males were mated with C57BL/6J females to produce mice heterozygous at the *Mfrn2* locus ($Mfrn2^{floxneo/+}$). The neomycin-resistance cassette was subsequently excised by recombination of FRT sites by breeding $Mfrn2^{floxneo/+}$ mice with *flp/flp* mice that express Flp recombinase under the Rosa26 promoter generating heterozygous $Mfrn2^{flox/+}$ animals. $Mfrn2^{flox/+}$ animals were mated with CMV-Cre recombinase mice to generate $Mfrn2^{+/-}$ animals.

Table 2
Mouse genotyping primers

Name	Sequence
M2probeF1	ATTTCTCCAGCTATCACTCTCGAG
M2probeF2	TTTCCTGCCTCTTATAGCTAAAGAG
M2probeR1	ACCCGGAGAGTCTGCCAGTTC
M2probeR2	TCTCTGTCCCAGTCCAGCTAG
Mito1-R7	AACCCCTCCTTAACCTTGGA
Mito1-F4	CCACAACCCCTTTGTTTCAT
Mito1-R9	GTCTCCGGCAGCTTAAAGTG
$MitO_2$-R	TCGAGTCGGTGGAAACCAATCT
$MitO_2$-F	AAGCTCTTCATTTCACAGAGAC
EXN4-100	CTGGGTGTTGAGCAGTGTTTT

$Mfrn2^{+/-}$ animals were mated to generate $Mfrn2^{-/-}$ animals. All animals were subsequently genotyped using primers for Mfrn1 and Mfrn2 as listed in Table 2 (Mito1-R7, Mito1-F4, Mito1-R9, Mito2-R, Mito2-F, and EXN4-100).

Animals

$Mfrn1^{flox/flox}$ mice were bred with $Mfrn2^{-/-}$ animals to generate $Mfrn1^{flox/flox}$ $Mfrn2^{-/-}$ homozygous animals, which were subsequently bred to *Alb-Cre* (Jackson Laboratory) to selectively inactivate *Mfrn1* in hepatocytes of $Mfrn2^{-/-}$ animals. In addition, $Mfrn2^{flox/flox}$ mice were bred to *Alb-Cre* (Jackson Laboratory) to selectively inactivate *Mfrn2* in hepatocytes. Tail DNA was subjected to PCR for genotyping along with specific tissues. All procedures involving animals were approved by the University of Utah Animal Care Committee. All mice were born and housed in the University of Utah transgenic facility or mouse house facility. Mice were maintained on a standard rodent chow of 350 mg/kg or low-iron chow 2-6 mg/kg (Harland, Teklad). For ALA experiments animals fed ALA in the drinking water for 6 weeks prior to liver porphyrin analyses (8).

Protoporphyrin IX, heme, and nonheme iron measurements

Liver was weighted and 100 mg mixed with water to ~200 μl in a microcentrifuge tube and sonicated for 12 cycles of 5-s intervals at 50% duty (~2.5 s on, 2.5 s off) using a microtip. A 50-μl aliquot was mixed vigorously with 200 μl of an extraction mixture of ethyl acetate (4 volumes) and glacial acetic acid (1 volume). The phases were separated by microcentrifugation for 1 min at maximum speed. The upper organic layer was immediately analyzed simultaneously for protoporphyrin IX and heme in the HPLC. For porphyrins, 80 μl of the sonicated cell homogenate was mixed with 80 μl of 3 M HCl, incubated at 37 °C for 1 h, and then microcentrifuged at maximum speed for 10 min. The supernatant was analyzed for porphyrins in the HPLC (45). For tissue and mitochondrial nonheme iron, tissues were weighed, 300 μl of TCA-HCl solution added, tissue was homogenized, and incubated at 65 °C for 20 h. Samples were centrifuged at 12,000 × *g* for 10 min, 10 μl of supernatant was transferred to 96-well–plates, 200 μl of Chromogen reagent (1% bathophenanthroline sulfonate/thioglycolic acid) was added, samples incubated 10 min and read at $OD_{535\ nm}$. Iron levels in samples were calculated using an iron reference (1 mg/ml, Fisher) standard curve.

Metabolomics

Metabolite extraction for LC–MS analysis—25-50 mg of each sample was suspended in 450 μl of cold ACN + 0.1 μg/ml of d_9-carnitine, d_9-tmao, and d_4-succinate internal standards and transferred into ceramic bead mill tubes (Omni International, Kennesaw, GA). Distilled water was added to each sample according to 50 μl − sample weight (mg). A process blank was prepared using only ACN and internal standards and 50 μl of water. Samples were processed in a bead mill for 30 s, then chilled at −20 °C for 1 h. Samples were then vortexed for 30 s. Samples were centrifuged at 20,000 × *g* for 10 min and the pellet discarded. The supernatant was transferred to fresh microcentrifuge tubes.

LC–MS analysis—50 μl of each sample, QC, and process blank solution was added to individual PTFE autosampler vials and randomized prior to analysis. An Agilent 6545 UPLC-QToF (Agilent Technologies, Inc., Santa Clara, CA) run in the positive mode was used for analysis. Separation was achieved using a Waters BEH amide 2.1 × 100-mm column with BEH amide pre-column (Waters Corporation, Milford, MA). An initial concentration of 99% ACN with 5% 10 mM NH_4OAc (A) and 1% 10 mM NH_4OAc in H_2O (pH 7, B) was held for 1.33 min. B was increased linearly to 30% at 5.13 min and again to 60% at 6.33 min. Finally, B was increased to 70% at 6.87 min and held for 2 min. Eluents were returned to starting conditions over 2 min. The system was allowed to re-equilibrate for 4 min between runs.

LC–MS data analysis—Data were collected using MassHunter software (Agilent). Metabolites were identified and their peak area was recorded using MassHunter Quant. These data were transferred to an Excel spread sheet (Microsoft, Redmond, WA). Metabolite identity was established using a combination of an in-house metabolite library developed using pure purchased standards and the METLIN library (RRID:SCR_010500). Further analysis was performed using Metaboanalyst4.0 (RRID:SCR_015539). To determine whether known metabolites were altered we used fold-change threshold = 1.5, *p* value threshold = 0.05; FDR-adjusted off.

ICP-MS

Mitochondria were isolated from livers of animals fed a low-iron diet for 10 weeks. Isolated mitochondria were subject to ICP-MS. Briefly, purified mitochondria were digested overnight in Optima 68% HNO_3 at room temperature, heated at 95 °C for 5 h until dry, and resuspended in 2% HNO_3 for analysis using an Agilent 7900 ICP-MS. Calibration standard solutions for determination of Fe, Zn, Co, Cu, and Mn were prepared from Agilent multielement calibration standard-2A. Protein concentrations of homogenates were determined by BCA Protein Assay (Thermo Fisher Scientific) for normalization.

Partial hepatectomy

Three-month–old female mice were subject to 2/3 partial hepatectomy as described (22). Forty-eight hours post-hepatectomy animals were sacrificed, livers were harvested and histologic examination was performed on pre- and posthepatectomized liver samples using Ki67 staining as a measure of cell proliferation.

Histology

Tissues were isolated from 3-month–old mice and fixed in formalin for a minimum of 24 h. Five-μm sections were generated and stained with H & E or Trichrome by AML Laboratories. Ki67 staining was performed at ARUP Laboratories, as previously described (22). Images were captured on an Olympus BX51 microscope (×10 objective) using QuantOne software. Positive Ki67 cells were quantified on blinded samples using animal numbers and not genotypes.

Cell culture and mitochondrial isolation

Fibroblasts were isolated from 3-month–old mouse skin (tail or armpit), grown in culture in Dulbecco's minimal essential medium (DMEM) with penicillin/streptomycin and 10% fetal bovine serum (FBS). Cells were immortalized by force through a senescence crisis. For localization studies, WT fibroblasts were transfected with pMfrn2-GFP or truncated Mfrn2-GFP and Mfrn1-mCherry. Twenty-four hours post-transfection cells were imaged using an Olympus BX51 microscope (×60 oil immersion objective with a 1.3 aperature) and QuantOne software. For deletion of the $Mfrn1^{flox/flox}$ allele cells were plated on 35-mm tissue culture plates, incubated with recombinant Tat-Cre for 1 h, growth medium was replaced, and cells were grown for 48 h. Genomic DNA or mRNA was prepared and PCR or qPCR were performed to confirm deletion of the $Mfrn1^{flox/flox}$ allele. Mouse hepatocyte isolation was performed as described (46, 47). Bone marrow-derived macrophages were isolated and grown as described (48). Tissue mitochondria were lysed in 1% octylphenoxypolyethoxyethanol, 0.1% SDS, 150 mM NaCl, 50 mM Tris-HCl, pH 7.2, 0.5 mM EDTA with 2× protease inhibitor mixture (Roche) and isolated as described (49). Cell culture mitochondria were isolated using the mitochondrial isolation kit from ThermoFisher (catalog number 89874).

Generation of $Mfrn1^{-/-}Mfrn2^{-/-}$ TET-LV-Tight.HuMFRN1-GFP fibroblasts

$Mfrn1^{f/f}Mfrn2^{-/-}$ fibroblasts were transduced with two vectors, LV-TetOff and pLV-Tight.HuMFRN1-GFP. The plasmids and viral vectors for the TET-regulated human mitoferrin1-GFP lentiviral system were generated and provided by the CCEH Vector Core at the Fred Hutchinson, Seattle, WA, essentially as described previously (50). Transduced cells were sorted for GFP expression and a stable line generated by selection in puromycin. HuMfrn1-GFP mitochondrial localization was confirmed by epifluorescence microscopy. Cells were treated with recombinant Tat-Cre to delete the chromosomal floxed allele of mouse *Mfrn1*, clones were isolated (No. 44 and 50) and deletion of *Mfrn1* confirmed by PCR.

RNA isolation, RNA-Seq, and RT-qPCR

For RT-qPCR, tissues were homogenized in TRIzol reagent and stored at −80 °C prior to RNA isolation. mRNA was extracted using the RNeasy kit from Qiagen. Two μg of total mRNA was used to synthesize cDNA using the High Capacity cDNA Reverse Transcription kit (AB Biosystems). Power SYBR Green Master mix (Life Technologies) was used on a Realplex2

Table 3
Primers for qPCR

Gene		Primer Sequence	Reference
B-Actin	Forward	GACGGCCAAGTCATCACTATTG	This study
	Reverse	CCACAGGATTCCATACCCAAGA	This study
Mfrn1	Forward	TTGAATCCAGATCCCAAAGC	This study
	Reverse	GTTTCCTTGGTGGCTGAAAA	This study
Mfrn2	Forward	TCGTCAAGCAGAGGATGCAGAT	This study
	Reverse	GTTAAAGTGCTCTTGCAGGAAC	This study
HIF2a	Forward	CTGAGGAAGGAGAAATCCCGT	This study
	Reverse	TGTGTCCGAAGGAAGCTGATG	This study
Atp2b2	Forward	AAAGAGAAGTCGGTGCTTCAG	This study
	Reverse	GTGTGCATTCCGTCAGCCA	This study
Slc30a1	Forward	GGAAGCGGAAGACAACAGGG	This study
	Reverse	CAAGGCATTCACGACCACG	This study
Slc39a5	Forward	ATCATCTGCTGACTGGCCTAT	This study
	Reverse	CAGTGTCCCGTTCTCTCCATA	This study
Slc39a14	Forward	GTGTCTCACTGATTAACCTGGC	This study
	Reverse	AGAGCAGCGTTCCAATGGAC	This study
Cebpe	Forward	CGCATTATGGAGACTCAGCA	This study
	Reverse	GCGCAGAGTGTCTAGCTCCT	This study
	Forward	CTGGGGAAGAACAGCTACTTTC	PrimerBank
	Reverse	GTGAGGGATAGGCGAATGGC	PrimerBank
Cyp3a44	Forward	GGGTCAATGGTGATGATTCC	This study
	Reverse	CCAATTCCAAAGGGCAGATA	This study
Enpp6	Forward	CAGAGAGATTGTGAACAGAGGC	PrimerBank
	Reverse	CCGATCATCTGGTGGACCT	PrimerBank

thermal cycler (Eppendorf). β-Actin was used as a control housekeeping gene. The $\Delta\Delta C_t$ method was used to compare the variation of transcripts among samples. Specificity and efficiency were checked before using this method. Primers were validated by cloning and sequencing the PCR products. Primers used in this study are listed in Table 3. RNA-Seq was performed on livers from 3 WT and 5 Alb-Cre*Mfrn1*$^{-/-}$*Mfrn2*$^{-/-}$ animals using the Illumina Platform. Data were analyzed using differential expression analysis and heat maps generated at the University of Utah Huntsman Cancer Institute Genomics/Bioinformatics core. The RNA-Seq data has been deposited in the National Center for Biotechnology Information under accession number GSE143925. Genes with multiple testing corrected p values < 0.05 were used in Ingenuity Pathway Analysis and Gene Set Enrichment Analysis (GSEA).

Other procedures

Blood was collected from anesthetized animals by retro-orbital eye bleed into heparinized tubes containing anticoagulant citrate dextrose. Hematocrit, hemoglobin, RBC numbers, and mean corpuscular volume were measured. Protein determinations were performed with BCA kit (Pierce). 50 μg of whole cell lysate or mitochondrial lysate with Laemmli buffer was heated to 65 °C for 20 min and run on 4–20% Tris glycine SDS-PAGE. Western blotting was performed using the following primary antibodies: rabbit anti-VDAC (1:1000, Abcam), mouse anti-OXPHOS (1:1000, Abcam), rabbit anti-Mfrn1 (1:2000), rabbit anti-GAPDH (1:1000, Thermo Fisher), rabbit anti-GFP (1:2000, GeneTex), rabbit anti-catalase (1:1000, Abcam), and either horseradish peroxidase-conjugated goat anti-rabbit or goat anti-mouse IgG (1:10,000, Jackson ImmunoResearch Laboratory). Western blots were developed using Western Lightning reagent (PerkinElmer Life Sciences). Aconitase activity was assayed as previously described (29). Xanthine oxidase was performed using the Amplex Red xanthine oxidase assay kit from Thermo Fisher. Complex I activity was assayed using Cayman MitoCheck activity kits (Caymen Chemicals).

Statistical analysis

Results were analyzed comparing single variables of either genotype or diet using a paired Student's t test. Significance was noted at: *, $p < 0.05$; **, $p < 0.01$; ***, $p < 0.001$; ****, $p < 0.0001$. Data are presented as mean ± S.D. or S.E. where stated in the legends.

Data availability

All data are contained within the manuscript with the exception of the complete RNA Sequencing data set, which is deposited in the National Center for Biotechnology Information (GSE143925).

Acknowledgments—We thank the Ward and Barasch labs for critically reading the manuscript.

Author contributions—A. S., A. Q., M-B. T., J. K., J. B., and D. M. W. conceptualization; A. S., X. J., A. M. E., L. L., J. W., A. Q., T. B., R. S., D. E. W., P. T. D., and D. M. W. data curation; A. S., L. L., J. W., A. Q., J. D. P., J. K., B. H. P., and D. M. W. formal analysis; A. S. and D. M. W. validation; A. S. and D. M. W. investigation; A. S. visualization; A. S., X. J., L. L., M. H., S. T., M. E. W., E. H., M. A. F., and D. M. W. methodology; A. S., X. J., A. M. E., L. L., J. W., A. Q., T. B., R. S., M-B. T., M. H., S. T., D. E. W., P. T. D., M. E. W., E. H., M. A. F., J. D. P., J. K., J. B., and D. M. W. writing-review and editing; M. E. W. resources; J. B. and D. M. W. funding acquisition; D. M. W. supervision; D. M. W. writing-original draft; D. M. W. project administration.

Funding and additional information–This work was supported by the National Institutes of Health Grant DK052830 (to D. M. W.), Grants R01DK073462 and R01DK092684 (to J. B.), U54DK110858

(to J. D. P. and D. M. W.), Grants DK070838 and P01 HL032262 (to B. H. P.) (deceased), University of Utah Pathology Seed Grant 28349 (to D. M. W.), and Grant U54DK106829 (to M. E. W. and B. Torok-Storb.) from the Co-operative Center of Excellence in Hematology. The content is solely the responsibility of the authors and does not necessarily represent the official views of the National Institutes of Health.

Conflict of interest—The authors declare no competing interests.

Abbreviations—The abbreviations used are: SLC, solute carrier; CMV, cytomegalovirus; ES, embryonic stem; ICP-MS, inductively coupled plasma mass spectrometry; qPCR, quantitative PCR; ALA, aminolevulenic acid; OXPHOS, oxidative phosphorylation protein; BMDM, bone marrow-derived macrophage; CSFE, carboxyfluorescein succinimidyl ester; FAC, ferric ammonium citrate; VDAC, voltage-dependent anion channels; Cebp, CCAAT enhancer-binding protein; DKO, double knockout.

References

1. Palmieri, F. (2014) Mitochondrial transporters of the SLC25 family and associated diseases: a review. *J. Inherit. Metab. Dis.* **37,** 565–575 CrossRef Medline
2. Puccio, H., Simon, D., Cossee, M., Criqui-Filipe, P., Tiziano, F., Melki, J., Hindelang, C., Matyas, R., Rustin, P., and Koenig, M. (2001) Mouse models for Friedreich ataxia exhibit cardiomyopathy, sensory nerve defect and Fe-S enzyme deficiency followed by intramitochondrial iron deposits. *Nat. Genet.* **27,** 181–186 CrossRef Medline
3. Rouault, T. A., and Tong, W. H. (2008) Iron-sulfur cluster biogenesis and human disease. *Trends Genet.* **24,** 398–407 CrossRef Medline
4. Chen, W., Paradkar, P. N., Li, L., Pierce, E. L., Langer, N. B., Takahashi-Makise, N., Hyde, B. B., Shirihai, O. S., Ward, D. M., Kaplan, J., and Paw, B. H. (2009) Abcb10 physically interacts with mitoferrin-1 (Slc25a37) to enhance its stability and function in the erythroid mitochondria. *Proc. Natl. Acad. Sci. U.S.A.* **106,** 16263–16268 CrossRef Medline
5. Hung, H. I., Schwartz, J. M., Maldonado, E. N., Lemasters, J. J., and Nieminen, A. L. (2013) Mitoferrin-2-dependent mitochondrial iron uptake sensitizes human head and neck squamous carcinoma cells to photodynamic therapy. *J. Biol. Chem.* **288,** 677–686 CrossRef Medline
6. Paradkar, P. N., Zumbrennen, K. B., Paw, B. H., Ward, D. M., and Kaplan, J. (2009) Regulation of mitochondrial iron import through differential turnover of mitoferrin 1 and mitoferrin 2. *Mol. Cell Biol.* **29,** 1007–1016 CrossRef Medline
7. Shaw, G. C., Cope, J. J., Li, L., Corson, K., Hersey, C., Ackermann, G. E., Gwynn, B., Lambert, A. J., Wingert, R. A., Traver, D., Trede, N. S., Barut, B. A., Zhou, Y., Minet, E., Donovan, A., *et al.* (2006) Mitoferrin is essential for erythroid iron assimilation. *Nature* **440,** 96–100 CrossRef Medline
8. Troadec, M. B., Warner, D., Wallace, J., Thomas, K., Spangrude, G. J., Phillips, J., Khalimonchuk, O., Paw, B. H., Ward, D. M., and Kaplan, J. (2011) Targeted deletion of the mouse Mitoferrin1 gene: from anemia to protoporphyria. *Blood* **117,** 5494–5502 CrossRef Medline
9. Bashir, K., Ishimaru, Y., Shimo, H., Nagasaka, S., Fujimoto, M., Takanashi, H., Tsutsumi, N., An, G., Nakanishi, H., and Nishizawa, N. K. (2011) The rice mitochondrial iron transporter is essential for plant growth. *Nat. Commun.* **2,** 322 CrossRef Medline
10. Ren, Y., Yang, S., Tan, G., Ye, W., Liu, D., Qian, X., Ding, Z., Zhong, Y., Zhang, J., Jiang, D., Zhao, Y., and Lu, J. (2012) Reduction of mitoferrin results in abnormal development and extended lifespan in *Caenorhabditis elegans*. *PLoS ONE* **7,** e29666 CrossRef Medline
11. Metzendorf, C., Wu, W., and Lind, M. I. (2009) Overexpression of *Drosophila* mitoferrin in l(2)mbn cells results in dysregulation of Fer1HCH expression. *Biochem. J.* **421,** 463–471 CrossRef Medline
12. Metzendorf, C., and Lind, M. I. (2010) The role of iron in the proliferation of *Drosophila* l(2) mbn cells. *Biochem. Biophys. Res. Commun.* **400,** 442–446 CrossRef Medline
13. Foury, F., and Roganti, T. (2002) Deletion of the mitochondrial carrier genes MRS3 and MRS4 suppresses mitochondrial iron accumulation in a yeast frataxin-deficient strain. *J. Biol. Chem.* **277,** 24475–24483 CrossRef Medline
14. Múhlenhoff, U., Stadler, J. A., Richhardt, N., Seubert, A., Eickhorst, T., Schweyen, R. J., Lill, R., and Wiesenberger, G. (2003) A specific role of the yeast mitochondrial carriers MRS3/4p in mitochondrial iron acquisition under iron-limiting conditions. *J. Biol. Chem.* **278,** 40612–40620 CrossRef Medline
15. Gutiérrez-Aguilar, M., and Baines, C. P. (2013) Physiological and pathological roles of mitochondrial SLC25 carriers. *Biochem. J.* **454,** 371–386 CrossRef Medline
16. Chen, Y. C., Wu, Y. T., and Wei, Y. H. (2015) Depletion of mitoferrins leads to mitochondrial dysfunction and impairment of adipogenic differentiation in 3T3-L1 preadipocytes. *Free Radic. Res.* **49,** 1285–1295 CrossRef Medline
17. Llorens, J. V., Metzendorf, C., Missirlis, F., and Lind, M. I. (2015) Mitochondrial iron supply is required for the developmental pulse of ecdysone biosynthesis that initiates metamorphosis in *Drosophila melanogaster*. *J. Biol. Inorg. Chem.* **20,** 1229–1238 CrossRef Medline
18. Grillo, A. S., SantaMaria, A. M., Kafina, M. D., Cioffi, A. G., Huston, N. C., Han, M., Seo, Y. A., Yien, Y. Y., Nardone, C., Menon, A. V., Fan, J., Svoboda, D. C., Anderson, J. B., Hong, J. D., Nicolau, B. G., *et al.* (2017) Restored iron transport by a small molecule promotes absorption and hemoglobinization in animals. *Science* **356,** 608–616 CrossRef Medline
19. Hare, J. F., and Hodges, R. (1982) Turnover of mitochondrial inner membrane proteins in hepatoma monolayer cultures. *J. Biol. Chem.* **257,** 3575–3580 Medline
20. Moullan, N., Mouchiroud, L., Wang, X., Ryu, D., Williams, E. G., Mottis, A., Jovaisaite, V., Frochaux, M. V., Quiros, P. M., Deplancke, B., Houtkooper, R. H., and Auwerx, J. (2015) Tetracyclines disturb mitochondrial function across eukaryotic models: a call for caution in biomedical research. *Cell Rep.* **10,** 1681–1691 CrossRef Medline
21. Fausto, N., Campbell, J. S., and Riehle, K. J. (2006) Liver regeneration. *Hepatology* **43,** S45–53 CrossRef Medline
22. Mitchell, C., and Willenbring, H. (2008) A reproducible and well-tolerated method for 2/3 partial hepatectomy in mice. *Nat. Protoc.* **3,** 1167–1170 CrossRef Medline
23. Serwas, N. K., Huemer, J., Dieckmann, R., Mejstrikova, E., Garncarz, W., Litzman, J., Hoeger, B., Zapletal, O., Janda, A., Bennett, K. L., Kain, R., Kerjaschky, D., and Boztug, K. (2018) CEBPE-mutant specific granule deficiency correlates with aberrant granule organization and substantial proteome alterations in neutrophils. *Front. Immunol.* **9,** 588 CrossRef Medline
24. Shyamsunder, P., Sankar, H., Mayakonda, A., Han, L., Nordin, H. B. M., Woon, T. W., Shanmugasundaram, M., Dakle, P., Madan, V., and Koeffler, H. P. (2018) CARD10, a CEBPE target involved in granulocytic differentiation. *Haematologica* **103,** 1269–1277 CrossRef Medline
25. Shyamsunder, P., Shanmugasundaram, M., Mayakonda, A., Dakle, P., Teoh, W. W., Han, L., Kanojia, D., Lim, M. C., Fullwood, M., An, O., Yang, H., Jizhong, S., Hossain, M. Z., Madan, V., and Koeffler, H. P. (2019) Identification of a novel enhancer of CEBPE essential for granulocytic differentiation. *Blood* **133,** 2507–2517 CrossRef
26. Studd, J. B., Yang, M., Li, Z., Vijayakrishnan, J., Lu, Y., Yeoh, A. E., Paulsson, K., and Houlston, R. S. (2019) Genetic predisposition to B-cell acute lymphoblastic leukemia at 14q11.2 is mediated by a CEBPE promoter polymorphism. *Leukemia* **33,** 1–14 CrossRef Medline
27. Zhang, Y. Y., Li, X., Qian, S. W., Guo, L., Huang, H. Y., He, Q., Liu, Y., Ma, C. G., and Tang, Q. Q. (2011) Transcriptional activation of histone H4 by C/EBPβ during the mitotic clonal expansion of 3T3-L1 adipocyte differentiation. *Mol. Biol. Cell* **22,** 2165–2174 CrossRef Medline
28. Nelson, D. M., Ye, X., Hall, C., Santos, H., Ma, T., Kao, G. D., Yen, T. J., Harper, J. W., and Adams, P. D. (2002) Coupling of DNA synthesis and histone synthesis in S phase independent of cyclin/cdk2 activity. *Mol. Cell Biol.* **22,** 7459–7472 CrossRef Medline
29. Li, L., and Kaplan, J. (2004) A mitochondrial-vacuolar signaling pathway in yeast that affects iron and copper metabolism. *J. Biol. Chem.* **279,** 33653–33661 CrossRef Medline

30. Yin, J., Xia, W., Wu, M., Zhang, Y., Huang, S., Zhang, A., and Jia, Z. (2019) Inhibition of mitochondrial complex I activity attenuates neointimal hyperplasia by inhibiting smooth muscle cell proliferation and migration. *Chem. Biol. Interact.* **304,** 73–82 CrossRef Medline
31. Diebold, L. P., Gil, H. J., Gao, P., Martinez, C. A., Weinberg, S. E., and Chandel, N. S. (2019) Mitochondrial complex III is necessary for endothelial cell proliferation during angiogenesis. *Nat. Metab.* **1,** 158–171 CrossRef Medline
32. Zhang, J., Pavlova, N. N., and Thompson, C. B. (2017) Cancer cell metabolism: the essential role of the nonessential amino acid, glutamine. *EMBO J.* **36,** 1302–1315 CrossRef Medline
33. Prado, F., and Aguilera, A. (2005) Partial depletion of histone H4 increases homologous recombination-mediated genetic instability. *Mol. Cell Biol.* **25,** 1526–1536 CrossRef Medline
34. Christenson, E. T., Gallegos, A. S., and Banerjee, A. (2018) *In vitro* reconstitution, functional dissection, and mutational analysis of metal ion transport by mitoferrin-1. *J. Biol. Chem.* **293,** 3819–3828 CrossRef Medline
35. Weisend, C. M., Kundert, J. A., Suvorova, E. S., Prigge, J. R., and Schmidt, E. E. (2009) Cre activity in fetal albCre mouse hepatocytes: utility for developmental studies. *Genesis* **47,** 789–792 CrossRef Medline
36. Zorn, A. M. (2008) Liver development. in *StemBook*. The Stem Cell Research Community, Cambridge, MA CrossRef
37. Hopkinson, B. M., Desler, C., Kalisz, M., Vestentoft, P. S., Juel Rasmussen, L., and Bisgaard, H. C. (2017) Bioenergetic changes during differentiation of human embryonic stem cells along the hepatic lineage. *Oxid. Med. Cell Longev.* **2017,** 5080128 CrossRef Medline
38. Li, L., and Kaplan, J. (2004) A mitochondrial-vacuolar signaling pathway in yeast that affects iron and copper metabolism. *J. Biol. Chem.* **279,** 33653–33661 CrossRef Medline
39. Kumfu, S., Chattipakorn, S., Fucharoen, S., and Chattipakorn, N. (2012) Mitochondrial calcium uniporter blocker prevents cardiac mitochondrial dysfunction induced by iron overload in thalassemic mice. *Biometals* **25,** 1167–1175 CrossRef Medline
40. Sripetchwandee, J., KenKnight, S. B., Sanit, J., Chattipakorn, S., and Chattipakorn, N. (2014) Blockade of mitochondrial calcium uniporter prevents cardiac mitochondrial dysfunction caused by iron overload. *Acta Physiol.* **210,** 330–341 CrossRef
41. Sripetchwandee, J., Sanit, J., Chattipakorn, N., and Chattipakorn, S. C. (2013) Mitochondrial calcium uniporter blocker effectively prevents brain mitochondrial dysfunction caused by iron overload. *Life Sci.* **92,** 298–304 CrossRef Medline
42. Froschauer, E. M., Rietzschel, N., Hassler, M. R., Binder, M., Schweyen, R. J., Lill, R., Mühlenhoff, U., and Wiesenberger, G. (2013) The mitochondrial carrier Rim2 co-imports pyrimidine nucleotides and iron. *Biochem. J.* **455,** 57–65 CrossRef Medline
43. Di Noia, M. A., Todisco, S., Cirigliano, A., Rinaldi, T., Agrimi, G., Iacobazzi, V., and Palmieri, F. (2014) The human SLC25A33 and SLC25A36 genes of solute carrier family 25 encode two mitochondrial pyrimidine nucleotide transporters. *J. Biol. Chem.* **289,** 33137–33148 CrossRef Medline
44. Yoon, H., Zhang, Y., Pain, J., Lyver, E. R., Lesuisse, E., Pain, D., and Dancis, A. (2011) Rim2, a pyrimidine nucleotide exchanger, is needed for iron utilization in mitochondria. *Biochem. J.* **440,** 137–146 CrossRef Medline
45. Yien, Y. Y., Robledo, R. F., Schultz, I. J., Takahashi-Makise, N., Gwynn, B., Bauer, D. E., Dass, A., Yi, G., Li, L., Hildick-Smith, G. J., Cooney, J. D., Pierce, E. L., Mohler, K., Dailey, T. A., Miyata, N., *et al.* (2014) TMEM14C is required for erythroid mitochondrial heme metabolism. *J. Clin. Invest.* **124,** 4294–4304 CrossRef Medline
46. Severgnini, M., Sherman, J., Sehgal, A., Jayaprakash, N. K., Aubin, J., Wang, G., Zhang, L., Peng, C. G., Yucius, K., Butler, J., and Fitzgerald, K. (2012) A rapid two-step method for isolation of functional primary mouse hepatocytes: cell characterization and asialoglycoprotein receptor based assay development. *Cytotechnology* **64,** 187–195 CrossRef Medline
47. Zhang, A. S., Xiong, S., Tsukamoto, H., and Enns, C. A. (2004) Localization of iron metabolism-related mRNAs in rat liver indicate that HFE is expressed predominantly in hepatocytes. *Blood* **103,** 1509–1514 CrossRef Medline
48. Paradkar, P. N., De Domenico, I., Durchfort, N., Zohn, I., Kaplan, J., and Ward, D. M. (2008) Iron depletion limits intracellular bacterial growth in macrophages. *Blood* **112,** 866–874 CrossRef Medline
49. Parsons, D. F., Williams, G. R., and Chance, B. (1966) Characteristics of isolated and purified preparations of the outer and inner membranes of mitochondria. *Ann. N.Y. Acad. Sci.* **137,** 643–666 CrossRef Medline
50. Zufferey, R., Nagy, D., Mandel, R. J., Naldini, L., and Trono, D. (1997) Multiply attenuated lentiviral vector achieves efficient gene delivery *in vivo*. *Nat. Biotechnol.* **15,** 871–875 CrossRef Medline